Article

Optimized Green Nanoemulsions to Remove Pharmaceutical Enoxacin from Contaminated Bulk Aqueous Solution

Afzal Hussain,* Syed Sarim Imam, Mohammad A. Altamimi, Mudassar Shahid, and Osamah Abdulrahman Alnemer
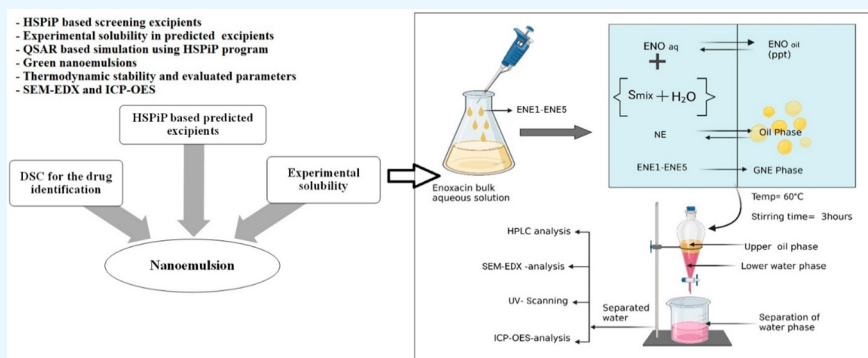
Read Online

ACCESS | Metrics & More | Article Recommendations | Supporting Information

ABSTRACT: We attempted to develop green nanoemulsions (ENE1−ENE5) using capryol-C90 (C90), lecithin, Tween 80, and N-methyl-2-pyrrolidone (NMP). HSPiP software and experimentally obtained data were used to explore excipients. ENE1−ENE5 nanoemulsions were prepared and evaluated for in vitro characterization parameters. An HSPiP based QSAR (quantitative structure−activity relationship) module established a predictive correlation between the Hansen solubility parameter (HSP) and thermodynamic parameters. A thermodynamic stability study was conducted under stress conditions of temperature (from −21 to 45 °C) and centrifugation. ENE1−ENE5 were investigated for the influence of size, viscosity, composition, and exposure time on emulsification (5−15 min) on %RE (percent removal efficiency). Eventually, the treated water was evaluated for the absence of the drug using electron microscopy and optical emission spectroscopy. HSPiP program predicted excipients and established the relationship between enoxacin (ENO) and excipients in the QSAR module. The stable green nanoemulsions ENE−ENE5 possessed the globular size range of 61−189 nm, polydispersity index (PDI) of 0.1−0.53, viscosity of 87−237 cP, and ζ potential from −22.1 to −30.8 mV. The values of %RE depended upon the composition, globular size, viscosity, and exposure time. ENE5 showed %RE value as 99.5 ± 9.2% at 15 min of exposure time, which may be due to the available maximized adsorption surface. SEM-EDX (scanning electron microscopy−X-ray dispersive energy mode) and inductively coupled plasma−optical emission spectroscopy (ICP-OES) negated the presence of ENO in the treated water. These variables were critical factors for efficient removal of ENO during water treatment process design. Thus, the optimized nanoemulsion can be a promising approach to treat water contaminated with ENO (a potential pharmaceutical antibiotics).

INTRODUCTION

Enoxacin (ENO) is a third generation antibiotic used to control bacterial infections without cross-resistance between other antibiotics.[1−3] Liu et al. attempted to develop a cocrystal of ENO with organic salt as an alternative strategy to liposomal and nanoparticle (with high precipitation). However, the salt was considered to be the least stable, which is not conducive to storage and transport.[4] Structurally, ENO contains H-bond donor and H-bond acceptor counts as 2 and 8, respectively. Being slightly acidic in nature of ENO, free −COOH (carboxylic acid), F-atom, N-heteroatom, O-atom, and a good electronic conjugation system are responsible for
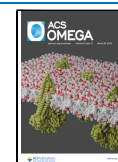
intermolecular H-bonding, $\pi−\pi$ stacking, and charge assisted H-bonding.[4]
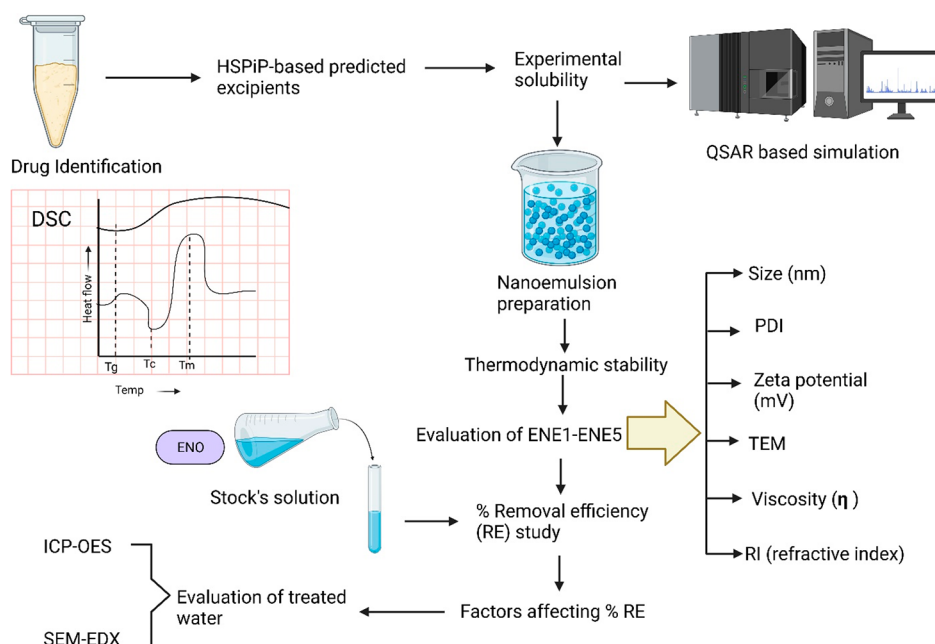
For the past few decades, exhaustive use of pharmaceutical antibiotics has become a global threat for human health and ecosystem (aquatic system and agriculture). This can be correlated with the total sale of antibiotics (82 tons) in 2011 as

Figure 1. Illustrative presentation of the experimental design to complete the proof of concept.

reported in the EMA (European Medical Agency) report as compared to global consumption (40.1 billions) of antibiotics in 2018.[5,6] Fluoroquinolones are broad spectrum antibiotics to treat animal and human diseases and have been detected in untreated and treated wastewater. The U.S. Geological Survey (USGS) reported approximately 0.12 μg/L of fluoroquinolones in several streams throughout the USA.[7] This level was globally high (0.15−0.3 mg/L) for ENO in India (Patancheru, Hyderabad) indicating the impact of several factors (anthropogenic, shortage of centralized sewage system, and direct discharge of sewage to river, canal, groundwater, soil, and surface water) responsible for contaminating water systems.[8] In 2017, Zhang et al. investigated the occurrence, level, removal efficiency, and risk assessment of 31 antibiotics from 12 different wastewater treatment plants in Dalian of China. These authors reported 29 antibiotics with an occurrence level range of 63.6−5404.6 ng/L in wastewater samples wherein 42.2% were fluoroquinolones.[9] Larsson et al. reported six (ofloxacin > norfloxacin > ENO > ciprofloxacin > enrofloxacin > other) out of 11 antibiotics in mg/L suggesting the highest level of water contamination with ENO in India.[8] Notably, the reported occurrence level of fluoroquinolones in the influents and effluents of wastewater were in the ranges of 2.0−8000 ng/L and 0.3−31000 ng/L globally, respectively.[9,10] The global regulatory agencies strictly asked that enough new ecotoxicological data and the fate of drug metabolism (photodegradation and hydrolysis) be provided before approving any product in their giudelines.[11−13] Municipal sewage, domestic outflow, industrial waste release, sewage from hospitals, and wastewater outflow from livestock of animal farming are the main sources of pharmaceutical contaminant for frequent emergence of antibiotic resistance and chronic toxicity in aquatic lives, humans, and plants.[11,12]

Several conventional techniques are associated with certain challenges. These are membrane filtration, reverse osmosis (RO), UV−H$_2$O$_2$ based photolysis, sonochemical degradation techniques, chlorination, ozonation, adsorption methods, and biodegradation method.[14−17] Nanofiltration (nanofilter) and

RO methods are related to foul smelling and physiological malfunctioning due to a present oxidizing agent. The most common technique "chlorination" is related to serious toxicity due to formed chlorinated byproducts.[18,19] Conventional adsorption based water treatment techniques are associated with various limitations (low removal efficiency, nonselectivity, hectic and time consuming concerns, costliness, low scalability, high maintenance issues, and low affinity of few drugs to the adsorbents such as activated charcoal).[20]

We established and reported various green nanoemulsions to remove active pharmaceuticals considered as the most serious contaminants so far with high removal efficiency, simplicity, ease to scale up, and specificity.[21−24] Considering the physicochemical properties of the drug, poor aqueous solubility (0.29 mg/mL an experimental value), low molecular weight (320.32 g/mol), weak acidic nature (pK_a = 5.5), and H-bond-forming ability, green nanoemulsion development using medium chain triglycerides and surfactants is an encouraging strategy to eliminate the trace amount of ENO released from influent or effluent water.[14] The method is simple, rapid, and economical. Therefore, we investigated the prospective excipients close to the drug for maximum solubility using Hansen solubility software (HSPiP software version 5.0.06). The program helps to predict suitable solvents, surfactants, cosurfactants, and lipids based on Hansen functional parameters. These parameters are based on the total cohesive energy as Hansen space (δ) distributed over dispersive force (expressed as δ_d), polarity (as δ_p due to dipole−dipole value), and hydrogen bonding forming ability (expressed as δ_h). Mathematically, Hansen space can be expressed as in eq 1:

$$\delta^2 = (\delta_d)^2 + (\delta_p)^2 + (\delta_h)^2 \tag{1}$$

The program assisted in screening excipients exhibiting a closeness between the drug and excipients in terms of interactive forces (polarity, dispersion, London forces, hydrogen bonding, and van der Waals) and their impact on the drug solubilization/miscibility, keeping other variables constant. The predicted excipients were used for the experimental

solubility study at 40 °C. Finally, the selected excipients were tailored into a green nanoemulsion. These were evaluated for size, polydispersity index (PDI), ζ potential, viscosity, morphology, stability, and refractive index (RI). Various factors were taken into account for having the impact on removal efficiency (%RE). Finally, instrumental techniques ensured the absence of ENO from the treated water. A complete methodology of the work is illustrated in Figure 1.

■ MATERIALS AND METHODS

Materials. Enoxacin (ENO, >99.6%) was a white crystalline powder and was obtained from Merck, Mumbai, India. PG (propylene glycol), IPM (isopropyl myristate), NMP (N-methyl-2-pyrrolidone), isopropyl alcohol (IPA), ethanol, ethyl acetate, ethyl lactate (EL), dimethyl isosorbide (DMI), and methanol, acetonitrile (ACN) were purchased from Merck. A few surfactants such as Tween 80 and triton-X-100 were procured from a local standard supplier of AR grade (Merck). Soybean oil was purchased from a local supplier (food grade) (Mr. Mohhammad Ramzan generously gifted, Chandigarh, Punjab, India). Capryol 90 (propylene glycol monocaprylate) (C90) was gifted from Gattefosse (France). Buffer reagents were purchased from Sigma-Aldrich, Mumbai, India. Distilled water was used as aqueous solvent.

Methods. *Thermal Behavior Analysis Using Differential Scanning Calorimeter (DSC).* The drug was subjected for thermal behavior using DSC (DSC-60, Shimadzu, Japan). The drug was weighed and transferred to a previously cleaned aluminum pan. The pan containing the same drug was completely crimped before placing into the furnace. The technique was used to assess fusion temperature and enthalpy values. The crimped drug was heated to 400 °C at the heating rate of 10 °C/min as per the method adopted before.[25] After completion of the maximum temperature, the system was cooled by purging with nitrogen gas (60 mL/min).[25,26]

Hansen Solubility Parameters (HSPs) Using HSPiP Program. Understanding dispersion/solubility properties of materials (carbon nanotubes, polymers, and quantum dots) and controlling solvent−solute interactions were widely used in industry for multiple purposes (pigment dispersion, paint, solubility, solvation, polymer adhesion, and textile coloration). Moreover, the tool has been explored for permeation of chemical across plastic (gloves for safety), skin (drug delivery), packing barriers (for food), and surface (paint purposes); Hansen solubility parameters are a well-known and established tool to predict interactions (dielectric constant, van der Waals, cohesive−adhesive force, and London forces) between a solute and solvent. These interactions are in the terms of thermodynamic parameters, cohesive forces, and other attractive forces. The total cohesive energy is distributed over dispersive force, polarity, and H-bonding force responsible for miscibility or solubility of a solute in a particular solvent. HSPiP program (HSPiP software version 5.0.06) was used to estimate these parameters for the drug, solvent, surfactant, and lipids. In the case of a mixture of lipids, we calculated it manually based on composition (%) and SMILES files. In the present study, we reported various HSP values for various excipients and the investigated drugs as per the method reported before.[27,28] These HSPs (Hansen space) are expressed as (a) δ_d, (b) δ_p, and (c) δ_h for dispersion power, polarity (due to dielectric constant), and H-bond formation of a solute in a specific solvent, respectively. These values are associated with physicochemical properties of a solute and solvent. Using the program, we estimated these values by putting SMILES data in respective input tab of HSPiP program. The software estimated δ_p, δ_d, δ_h, and δ_{total}, and R values, wherein the values of δ_{total} and R represent the total HSP and space parameter, respectively.[28]

Theoretically, these HSPs are used to predict possible degrees of interaction between solute and solvent at fixed temperature so that a formulator or researcher can screen the right solvent for maximized solubility. Thus, the minimum difference of any HSP parameter between the investigated solute and solvent can be taken as soluble/miscible (δ_{hsp} of a solute − δ_{hsp} of solvent ~ 0). A solvent is considered suitable for a solute with R (space parameter in term of distance or interactive radius) values less than or equal to the R value of the investigated solute ($R_{solvent} \leq R_{solute}$) in the solubility sphere (HSP sphere). R_s and R_v indicate the sphere radius and the space parameter of solvent, respectively, from the center of the same HSP sphere (H). RED (relative energy difference) is defined as the ratio R_s to R_v, which must be less than unity for miscibility (RED < 1) of the solute and varies depending upon the nature of the solvent and existing interactions between both and vice versa (RED > 1 for immiscible).

Experimental Solubility. HSPiP software predicted various suitable solvents, oils, and surfactants for maximum solubility of the drug. ENO is very poorly soluble in an aqueous system or buffer. A weighed amount of the drug was added to a glass vial containing solvent, and the vial was tightly closed. The vial was transferred to a shaking water bath (Remi Equipment, Mumbai, India) previously set at 40.0 ± 1 °C for 72 h for saturated solubility. The study was performed in triplicate for each excipient. At the achieved equilibrium, the mixer was centrifuged to remove undissolved drug content. The supernatant was used to assess the content of the drug dissolved. The drug was quantified using a validated HPLC (reverse phase high performance liquid chromatography) method at λ_{max} of 345 nm, and the method was adopted as per the method reported before (slightly modified).[29] The mobile phase was composed of acetonitrile and citric acid (0.05 M) buffer (pH = 4.0) in 20:80 ratio, and the analysis was carried out with flow rate, sample injection volume, and run time of 1 mL/min, 20 μL, and 10 min, respectively. The column (C$_{18}$ of Hypersil) was operated at 30 ± 1 °C. Experiment was performed in triplicate to get average data. The calibration concentration range and regression coefficient were 1.0−100 ng/mL and 0.999, respectively.

QSAR (Quantitative Structural Activity Relationship) Model Using HSPiP Program. This model was used to predict solvent and a blend solvent suitable for ENO. In this model, we used HSP parameters of ENO and target solvent or blend of solvents. Physicochemical properties of the drug and solvent(s) are responsible for the drug miscibility. The HSP of the drug, excipients, and experimental solubility values were used in QSAR analysis. The model correlated a relationship between log S (experimental solubility) and HSP (δ_d, δ_p, and δ_h) or mVol. The model also correlates with thermodynamic functional parameters (enthalpy, entropy, and Gibbs energy). The model identified a trend of solvent data set and predicted right solvent close to the HSP values of ENO followed by predicting the impact of factors (thermodynamic parameters, HSP parameters, and molar volume) on log S of the drug in the target solvent or blend.[30] The best fit of the model was validated by regression coefficient values. The "cross-term" indicates interaction properties.

Constructing Various Pseudo-ternary-phase Diagrams. After HSPiP program based estimated HSP values for each studied excipient, experimental solubility, and QSAR model, excipients were selected for developing green nanoemulsion. For this, lipid, cosurfactant (CS), and surfactant (S) were selected for tailoring GNEs (green nanoemulsions). Therefore, a slow emulsification and titration method was adopted to generate a pseudoternary phase diagram. Various GNEs were prepared with varied ratios of S/CS termed as "S_{mix}". Initially, water-in-oil based nanoemulsions were prepared for a particular S_{mix} value (1:1, 1:2, and 1:3). Varied ratios of S_{mix}-to-oil phase (1:9 to 9:1) were applied to formulate nano-emulsions.[22] A phase diagram possessing the maximum delineated area was selected as an optimized nanoemulsion with minimum content of surfactant with high stability.

Thermodynamic Stability Assessment of Nanoemulsions. This study was conducted to ensure the stability of nanoemulsions (ENE1−ENE5) against thermal (extremely low and extremely high) and physical stress (ultracentrifugation). Generally, the obtained nanoemulsions were screened based on the stable, unstable, and metastable forms. Unstable and metastable nanoemulsions were identified and removed from further studies. Therefore, each nanoemulsion was subjected to exposure of a cyclic process of extreme temperatures (4, −21, and 45 °C after incubation) and ultracentrifugation. In freeze−thaw cycles, there were three repetitions of cycles wherein the sample vial was stored at −21 °C for 24 h. Then, the sample was removed and placed undisturbed at room temperature (30 °C) to resume the original state (within 5 min). The sample was considered as thermodynamically stable if the state resumed within 5 min without signs of any physical instability. The resumed sample was again stored at high temperature 45 °C for the same time period. Then, it was removed to place at room temperature for physical observation. The same cycle pattern was adopted for intermediate temperature (4 °C) for the same sample. Finally, to negate physical instability, an ultracentrifugation step was performed at 30000g for 5 min followed by keeping for 24 h to observe benchtop stability.[31,32] Each sample was inspected after incubation and resumed transparency (clear and isotropic) of ENE1−ENE5 at room temperature (30 °C) after 30 min. They were expected to resume their original consistency and physical stability.

Evaluations of ENE1−ENE5. Nanoemulsions stable under the stress thermodynamic stability study were subjected to characterizations (particle size, ζ potential, polydispersity index, RI, η, and morphology.

Evaluations of Size, Polydispersity Index (PDI), and Real Time ζ Potential Values. The globular size, PDI, and ζ values were determined using a Malvern Zetasizer (Malvern Nano-ZS-90 Zetasizer, Worcestershire, U.K.). The ζ values were determined using undiluted samples, whereas the sample for size estimation was processed using a diluted sample (distilled water as diluent). In brief, a freshly prepared nanoemulsion was taken and diluted with distilled water (100 times) to avoid any scanning interference during analysis. The diluted sample was taken in the sample holder previously washed and cleaned. The sample holder was filled leaving a 25% empty space from the top. The sample was placed in the analysis slot in such a way that the transparent portion should face the beam of light coming from the source. The sample holder was properly wiped with tissue paper to avoid any fingerprints or adhered sample on the surface before putting in the sample slot.

Analysis was run at a scattering angle of 90° and 25 °C for each sample. The system was run in size analysis mode. The system scans multiple times to provide a mean value and intensity graph. The process was repeated for each sample. Therefore, the size findings estimated using DLS (dynamic light scattering) are the hydrodynamic diameter of the particle obtained through Stokes−Einstein eq 2. The method is suitable for small particles due to better scattering as compared to laser diffraction (suitable for larger particles).

$$D = \frac{KT}{6\pi\eta r} \tag{2}$$

wherein D indicates diffusion coefficient. K and T represent the Boltzmann constant and the absolute temperature, respectively. The dynamic viscosity and the globular size (in diameter) were expressed as η and r, respectively.

To measure ζ potential, the same instrument was used in ζ potential measuring mode. The sample holder is a folded capillary cell composed of polycarbonate (capacity of 0.75 mL). Notably, the sample was undiluted to find the tangible charge of the tested sample. The sample was first taken into a syringe (without needle). The test sample was then filled into the sample holder (the folded capillary cell) in such a way that there should be no retained bubble inside. Both ends of the sample holder were filled completely and closed with closures. To avoid any adherence of the sample outside on the surface, tissue paper or cotton was used to it wipe out. The cell was placed inside for 2−3 min to allow the temperature to equilibrate. Notably, the exposed metallic electrode must be dried. The system was run to analyze the sample. The laser Doppler electrophoresis measured the electrophoretic mobility (related to Henry law) of the dispersed nanoglobules in the aqueous system. The analysis was repeated for mean and standard deviations.

Transmission Electron Microscopy (TEM). TEM technique was used to investigate the shape and size of the nanoemulsion globules after dispersion in the aqueous system. For this each sample (ENE1−ENE5) was separately dispersed in the drug aqueous solution for 15 min. The dispersed sample was immediately used for TEM analysis. The sample was placed on the grid (carbon coated grid). The additional sample was removed by blotting paper. The sample was then stained (using 0.1% phosphatungstic acid) and dried in an oven at ambient temperature (30 °C) for 2 h. The sample was scanned under TEM. The final micrographs were recorded at different locations and magnifications.

Notably, the size obtained from the DLS method differs from that of the transmission electron microscopy based technique. This was obvious due to the different principle of working. In practice, the estimated size varies as per the method and technique adopted and considered as instrumental error (relatively small globules were preferentially more adsorbed by the grid surface than big particles). Thus, the difference is reported as "fold error" (FE) using eq 3 and considered as an acceptable difference if it comes to less than 2.[33]

$$FE = 10^{(1/n)\sum\log(size,\text{Zetasizer}/size,\text{TEM})} \tag{3}$$

where "n" is the number of repeats of the experimental study.

Determination of Viscosity (η). All developed green nanoemulsions were composed of water, oil, and S_{mix} in proper ratio. Therefore, it was mandatory to measure flow behavior (rheology parameter such as η) of ENE1−ENE5.

Viscosity is a thermophysical property of nanofluid which is imperative for the design, selection of variables, and operation of the instrument involved in water treatment (such as wastewater treatment plant). The parameter is associated with having a great impact on mixing, blending, flow, processing, pumping, emulsification, and storage of nanoemulsion. The values of viscosity were estimated using Bohlin viscometer (Bohlin Visco 88, Malvern).[34] The viscometer was coupled with a cone and plate coaxially arranged in the vertical position. The cone with shaft was fixed to the roof of the solid metallic. The flat plate was fixed to the plate form of the base. Using the software command, the cone was descended to come down near the plate at the bottom, leaving a minute gap (25 mm). A paper is allowed to pass through the gap to ensure the presence of the gap as per a fixed distance set in the input slot of the software. Now, all operating conditions are fed in the system before placing the sample in the gap. These operational conditions are rotational speed (0−1000 rpm), shear rate range (from zero to 0.1×10^4 per second), torque range (1 mN m), shear stress (100 Pa), operating voltage (9 V), and working temperature. The operational temperature was kept constant throughout the analysis process. The system was run on ascending and descending cycles for each sample. Each sample (1 g) was placed in the gap existing between them, and the spindle is allowed to rotate at constant rotation. The sample (undiluted) was processed at 25 °C with a shear rate of $0-100 \ s^{-1}$.[33,34] Analysis was replicated to get a mean value for each sample. During the sample analysis, the external temperature was kept constant (25 °C).

Measurement of Refractive index (RI). The values of RI were determined using an Abbe-type refractometer (Bausch and Lomb Optical Co., Rochester, NY, USA) for neat oil, water, and ENE1−ENE5. In brief, the sample (a drop) was kept on a glass slide and assessed at 25 ± 1 °C. In the literature, RI values of water and oil are 1.33, and 1.47, respectively, at 20.0 °C.[35] In general, nanoemulsions are considered as kinetically stable and transparent (refractive index ∼ 1.32).[36] The normalized RI difference "*X*" can be mathematically defined as eq 4:

$$X = \frac{(\eta_0 - \eta)}{\eta_0} \tag{4}$$

where η_0 and η are the RI values of the sample processed and neat water, respectively. It is noteworthy that the model is applied for clear and isotropic systems with globular size < the wavelength of visible light.

Preparation of Stock Solution. The drug is poorly soluble in water (0.29 mg/mL at 25 °C) and considered as the most serious pharmaceutical contaminant. Considering the lowest concentration of ENO in effluents and poor solubility, a stock solution was prepared by dissolving a weighed amount of ENO in distilled water; the final strength of the drug solution was 10.0 ppm. This served as the working standard at laboratory scale to simulate an industrial scale-up process. From the stock solution, a range of concentration was prepared to use as the calibration curve concentration (0.01−10.0 µg/mL). To observe the pH of the solution, a digital pH meter was employed at different time points. A working calibration curve was drawn using HPLC at 30 ± 1 °C (operating column temperature).

Adsorption Study in Terms of Removal Efficiency. ENO is a poor water-soluble antibiotic with slightly acidic nature (pK_a

= 5.5).[14] The drug has been reported to be degraded in aqueous solution (0.02 µg/mL) after irradiation of UV light.[14] Removal efficiency of ENO depends upon the physicochemical properties of the drug and excipients. Several other factors (hydrophobicity, globular size, viscosity, temperature, composition, HSP parameters, and time of exposure) are also considerable forces to have an impact on removal efficiency. In this study, pH (5.5) and temperature (25 °C) were kept constant throughout the study. Thus, the composition, viscosity, size, PDI, and time of exposure were taken into account for %RE study. It was anticipated that there may be facilitated migration/diffusion of ENO from aqueous solution (pH = 5.5) to the water−oil interface for adsorption through electrostatic interaction force.[37] In brief, a weighed amount (1 g) of ENE1−ENE5 was dropped into the aqueous stock solution (10 mL) and stirred for various time points (5−20 min). After dispersion, the water-in-oil (w/o) nanoemulsion (ENE1−ENE5) was transformed to respective oil-in-water (o/w) nanoemulsion (o/w type of ENE1−ENE5) due to phase inversion. This was performed for each nanoemulsion separately, and data were recorded accordingly. Sampling was conducted at each time point to characterize the newly formed respective nanoemulsions. Then, an ENO−ENE mixture was completely cracked (destabilized) after freezing (at −21.0 °C) the sample for 0.5 h and subsequently heating at 60 °C for 2.5 h. The sequential steps of extreme freezing and immediate heating at high temperature results in two phase separation. Both phases were carefully segregated using ultracentrifugation technique (25000 rpm for 5 min) for the drug quantification.[23] The study was repeated for three time points to identify the impact of time (5.0, 10.0, and 20.0 min) of exposure on %RE. Finally, the total concentration of ENO (X_t) was assayed at varied time points and expressed as "ppm/g" using eqs 3 and 4:

$$Q_t = [(X_0 - X_t)/w]V \tag{5}$$

Thus, %RE was calculated using eq 6:

$$\%RE = [(X_0 - X_t)/X_0] \times 100 \tag{6}$$

The X_t and X_0 indicate the concentration (ppm) of ENO at t and "zero" time points, respectively. Moreover, V, w, and m are the dispersed volume (mL), the total amount (g), and the mass of GNE (g), respectively.

Confirmation of the Treated Water for the Absence of ENO. SEM-EDX (Scanning Electron Microscopy−Energy Dispersive X-ray) Analysis. The technique is used to identify the elemental composition of the sample under SEM and quantitative composition information (particularly in percent and peak intensity). The study is a supportive investigation so that the finding can be further ensured by another sophisticated advanced technique. For this, a fine smear of the treated water was developed on a cleaned glass slide. The sample was allowed to dry so that any metal can remain on the surface if present. The method is suitable to identify the elemental contaminant on and within the material such as barium, potassium, strontium, and chlorine.[38] The elements (H and O) of water were nullified from quantitative analysis. This was conducted using the software to avoid interference in the result. The procedure was adopted as described in a previously reported method.[24] The coated specimen was visualized, localized, and focused on to take suitable images under SEM-EDX mode (JEOL, Tokyo, Japan). The content of the element was expressed in percent (peak intensity).

Elemental Analysis from the Treated Water. An advanced instrument ICP-OES (Thermo Fisher Scientific, Bremen, Germany) is well-known to investigate elements of an organic compound dissolved in water.[39] The technique is commonly used to analyze the ultratrace content of an element present in solution as minor, major, and trace elements. The principle of working involves the measurement of emitted light (a completely passive process). The method has been adopted for the simultaneous determination of metal and nonmetal elements present as toxic contaminants in dietary supplements.[40,41] Afzal et al. reported the application of ICP-OES to identify various heavy metals (Ni and Co) present in the treated water (microbial method of water treatment) from industrial effluent water.[42]

In brief, the treated water was collected and subjected for quantitative assessment of trace elements present in the sample. For this, ICP-OES was used to scan following a validated method. The process was repeated to measure the average content of dissolved elements present in the sample. The acceptable result was assessed as 5%. The working calibration curve was prepared using varied dilutions of the analytical standard (standard solution). Analysis was carried out at room temperature.

■ RESULT AND DISCUSSION

Exhaustive use of pharmaceutical antibiotics (enoxacin) raised a serious and global concern due to environmental pollution. ENO accounts for 17% of the global market in antibiotic consumption, and it is released from different sources to aquatic systems.[43] That is why the topic has attracted increasing attention among the scientific community. Conventional methods are challenged with poor removal efficiency, foul smelling, and other disadvantages. Green nanoemulsions have already been explored to remove pharmaceutical antibiotics from contaminated water in the literature (as discussed in the Introduction). However, Hansen solubility parameters based prediction for the selection of excipients, simulation of the experimental solubility using HSPiP program, and green nanoemulsion using lecithin and medium chain triglycerides have not been investigated to remove ENO from contaminated water so far. Figure 1 summarizes the experimental design to accomplish the proof of concept.

Thermal Assessment of ENO for Drug Identification. ENO is a solid quinolone antibiotics with theoretical melting point of 220−224 °C, molecular weight of 320 g/mol, and log $P = -0.2$.[44] The exhibited two prominent endothermic thermal peaks are shown in Supporting Information Figure S1. The first broad peak represents the moisture content in the sample which might be adsorbed during handling or storage. The second prime peak was obtained at 223.8 °C which can be related with the fusion temperature of ENO. The value is quite close to the theoretical melting point of ENO, confirming the purity of the sample. The thermal exposure continued until 300 °C to investigate the impact of higher temperature on the drug degradation. However, there was no observed recrystallization or degradation at temperature beyond the fusion temperature. The small thermal noise can be identified in the thermogram (Figure S1) which may be due to temperature fluctuation. Thus, the drug could not execute any polymorphism, drug degradation, and recrystallization at the studied temperature range.

HSPiP Software Based Predicted Excipients. As we mentioned about HSPiP software in the experimental section,

the purpose of using the software was to screen out suitable excipients such as oil, surfactant, and cosurfactant based on the physicochemical properties and the Hansen solubility parameters (HSP). These HSPs are based on the sum of the total cohesive energy (δ_{total}) arising from dispersiveness (δ_d), polar behavior (δ_p), and H-bonding formation capability (δ_h). Considering the structural behavior of ENO and other excipients, the basic understanding of H-bond acceptor groups and H-bond donor groups can be explained as well (Figure 2).
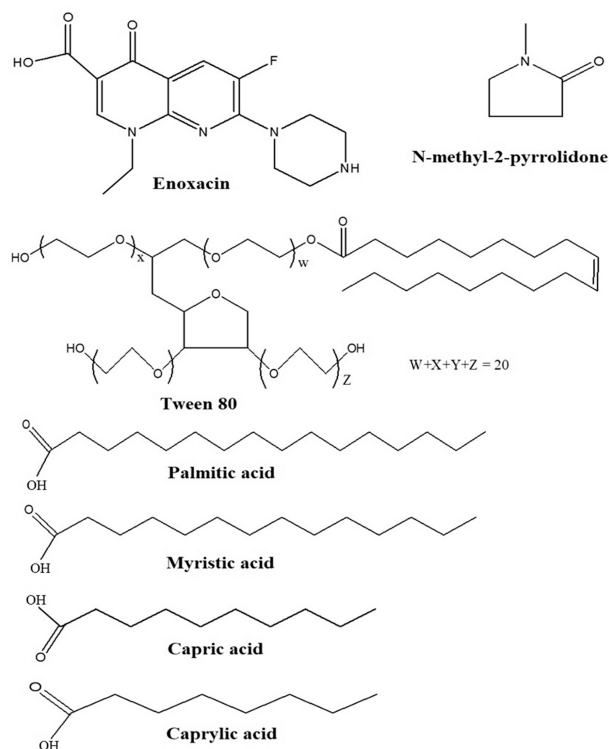
Figure 2. Chemical structures of the drug (enoxacin) and selected excipients (*N*-methyl-2-pyrrolidone, capric acid, caprylic acid, Tween 80, palmitic acid, and myristic acid).

A molecule can interact with another molecule in terms of polarity, H-bond formation ability, and dispersion ability.[28] These three basic HSP tools relate and predict the drug solubility in a particular solvent, oil, surfactant, and cosolvent. Therefore, the values of HSPs for the drug and various excipients have been presented in Table 1. To formulate a nanoemulsion, it was imperative to screen suitable oil, surfactant, and cosurfactant for the drug.

Table 1 provided detailed values of δ_d, δ_p, δ_h, δ_{total}, and R (space value) for ENO and components estimated from HSPiP program. It is obvious from Table 1 that the predicted values of δ_d, δ_p, δ_h, and δ_{total} for ENO were estimated as 19.2, 11.0, 9.7, and 24.1 MPa$^{1/2}$, respectively. Based on this, the drug is considered highly dispersive, polar, and capable to form H-bonding with excipients possessing approximate values of these estimated HSPs. Looking at the structure of ENO (Figure 2), the drug possessed 8 H-bond acceptor groups and 2 H-bond donor groups. This can be correlated with the predicted δ_h value of ENO (9.7 MPa$^{1/2}$). Theoretically, a solvent or cosolvent can be ideal for maximized miscibility of ENO if the difference of any HSP between ENO and solvent comes as zero or nearly zero (δ_d of ENO − δ_d of excipient ≈ 0; δ_p of ENO − δ_p of excipient ≈ 0; and δ_h of ENO − δ_h of excipient ≈

Table 1. Various Hansen Solubility Parameters of ENO and Screened Excipients for Maximum Solubility[a]

	Hansen solubility parameters					
Code	δ_d	δ_p	δ_h	δ_{total}	R value	SMILES
ENO	19.2	11.0	9.7	24.1	9.3	CCn1 cm³(c(=O)c2c1nc(c(c2)F)N3CCNCC3)C(=O)O
Transcutol-HP	16.3	7.4	12.0	21.6	5.2	CCOCCOCCO
Ethanol	15.6	9.3	17.2	25.0	8.49	CCO
Ethyl acetate	15.7	6.3	7.5	18.5	6.25	CCOC(=O)C
Tween 80	16.8	6.5	9.5	20.0	5.1	CCCCCCCCC=CCCCCCCCC(=O)OCCOCC(OCCO)C1OCC(OCCO)C1OCCO
DMI	17	13.5	27.4	35.5	18.01	CO[C@@H]1CO[C@H]2[C@@H]1OC[C@@H]2OC
PG	17.3	10.2	22.1	29.8	12.6	CC(CO)O
IPA	15.5	7.2	12.8	21.3	6.14	CC(C)O
NMP	17.9	9.9	7.4	21.8	2.86	CN1CCCC1=O
Triton X-100	16.8	3.9	6.7	18.5	8.1	CC(C)(C)CC(C)(C)c1ccc(cc1)OCCOCCO
Miglyol 812 N[b]	16.3	4.7	9.35	19.7	6.94	
Capric acid	16.3	4.2	8.6	18.9	7.47	CCCCCCCCC(=O)O
Caprylic acid	16.3	5.2	10.1	19.8	6.49	CCCCCCC(=O)O
IPM	16.15	4.7	6.22	19.09	7.8	CCCCCCCCCCCCC(=O)OC(C)C
Ethyl lactate	16.7	7.7	13.1	22.6	5.36	CCOC(=O)[C@H](C)O
Methanol	16.4	12.3	21.7	29.9	12.4	CO
Capryol 90[c]	18.35	5.1	9.8	21.4	5.96	
Soybean oil[d]	16.5	2.0	2.7	16.84	11.7	

[a]ENO, enoxacin; M812N, Miglyol 812 N (containing 50% caprylic acid and 50% capric acid); IPM, isopropyl myristate; DMI, dimethyl isosorbide; NMP, N-methyl-2-pyrrolidone; PG, propylene glycol; IPA, isopropyl alcohol; capryol 90 (propylene glycol monocaprylate), caprylic acid (90%), capric acid (3.0%), lauric acid (3.0%), myristic acid (3.0%), and palmitic acid (1.0%). [b]Manually calculated value based on 50% components of capric and caprylic acid in M812N. [c]Reference 46. [d]Reference 28.

0).[45] This solubility may be envisaged due to interactive forces (cohesive energies, H-bonding, dipole−dipole interaction, and dispersive nature) between ENO and excipient. Based on this, we compared the HSPs of the drug and each excipient (as shown in Table 2) for the right selection of excipients for tailoring the nanoemulsion.

Table 2. Composition of Various Green Water/T80/NMP/C90 Nanoemulsions at Fixed S_{mix} Ratio and HSP Parameters of ENE5 Based on Composition[a]

		Composition (% (w/w))			
Code	Water	TL	NMP	C90	S_{mix}
ENE1	3.5	15	45	36.5	1:3
ENE2	7.0	15	45	33.0	1:3
ENE3	10.5	15	45	29.5	1:3
ENE4	14.0	15	45	26.0	1:3
ENE5	17.5	15	45	22.5	1:3
HSP Parameters of ENE5 Based on Composition					
	Water	T80	NMP	C90	ENE5
δ_d	2.71	2.52	8.1	4.13	17.46
δ_p	2.8	0.975	4.46	1.15	9.385
δ_h	7.4	1.425	3.33	2.21	14.37
R_c (calculated)					6.04
δ_t	47.6	20	21.0		
RED (HSPiP)	3.63	NA	0.4	NA	NA

[a]TL, Tween 80 + lecithin; NMP, N-methyl-2-pyrrolidone; C90, capryol 90; NA, not available.

tailoring the nanoemulsion. The values of δ_d, δ_p, and δ_h for Tween 80 were estimated as 16.8, 6.5, and 9.5, respectively, indicating H-bonding ability and dispersive potential of Tween 80 could be prime factors for maximum miscibility of the drug. This can be further justified by the calculated difference values of HSP (δ_d of ENO − δ_d of Tween 80 = 2.4, δ_p of ENO − δ_p of Tween 80 = 4.5, and δ_h of ENO − δ_h of Tween 80 = 0.2). Thus, the least values of HSP difference between the solute

and Tween 80 were obtained for δ_d and δ_h. In the case of NMP, all three HSP parameters are prime determining factors for maximum miscibility/solubility of ENO as evidenced with the values of δ_d (17.9), δ_p (9.9), and δ_h (7.4) and their differences (δ_d of ENO − δ_d of NMP = 1.3, δ_p of ENO − δ_p of NMP = 1.1, and δ_h of ENO − δ_h of NMP = 1.3) with ENO. C90 is a mixture of various fatty acids as shown in Table 1. Therefore, HSP values were estimated manually based on the composition of the fatty acids and HSP values of the fatty acids. Thus, the values of δ_d, δ_p, and δ_h were calculated as 18.35, 5.1, and 9.8, respectively.[28,46] The values of difference of HSP between ENO and C90 were observed as 0.85, 5.9, and 0.1 for δ_d, δ_p, and δ_h, respectively [δ_d of ENO − δ_d of C90 = 19.2 − 18.35 = 0.85; δ_p of ENO − δ_p of C90 = 11.0 − 5.1 = 5.9; and δ_h of ENO − δ_h of C90 = 9.8 − 9.7 = 0.1]. Figure 3 depicted HSP values and HSP sphere of ENO as estimated in HSPiP software program. Figure 3A represents the solubility sphere of ENO and predicted solvents (inside and outside spheres) as a result of maximum interactions for ENO miscibility (black arrow indicated NMP as the most preferred solvent or cosolvent), whereas Figure 3B reveals a ternary diagram of HSP parameters and centralized ENO (R = 9.3). There are only three solvents within the sphere (r < 9.3). Thus, a solvent or excipient exhibiting an R value less than the drug (r) is considered as a suitable solvent for maximum miscibility/solubility.[47]

Therefore, Tween 80 (as surfactant), NMP (as cosolvent), and C90 (as lipid) were selected as excipients for nanoemulsion preparation which may exhibit maximized miscibility/solubility for ENO to remove from aqueous drug solution. In addition, experimental solubility of ENO in these predicted excipients further justified the selection process. Eventually, HSP parameters and experimental solubility values would decide which excipients to select before further study. There are limited solubility data available for ENO in various solvents and varied temperatures.
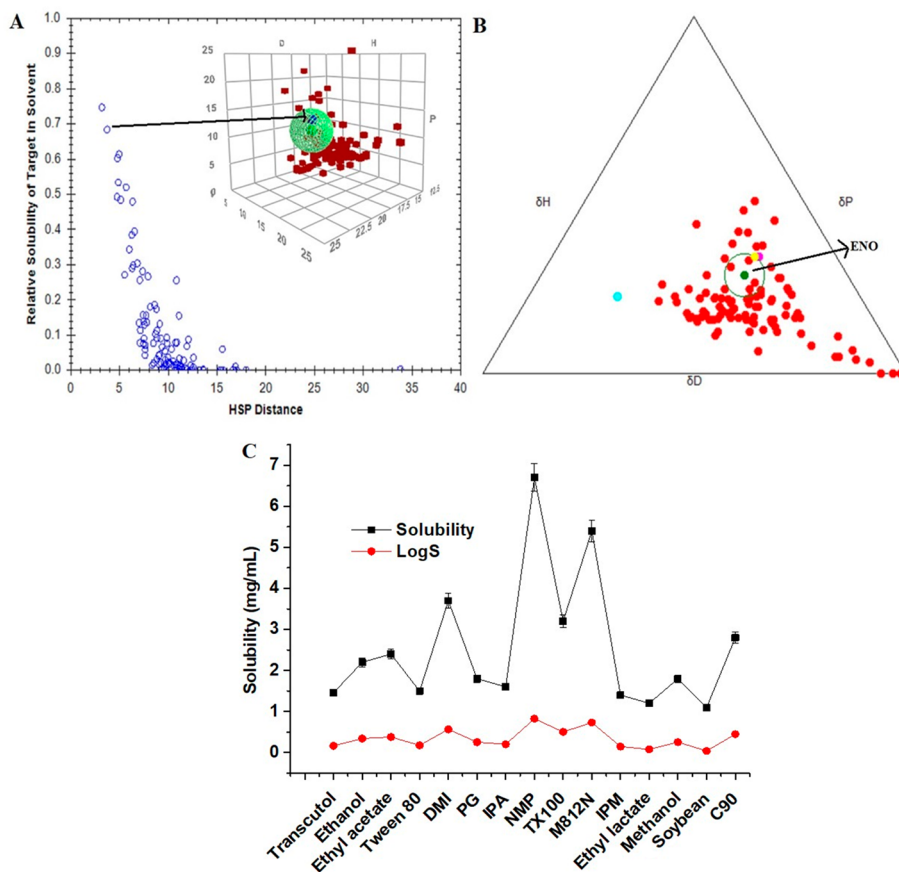
Figure 3. HSP values and HSP sphere of ENO in HSPiP software program: (A) Solubility sphere of ENO and predicted solvents (inside and outside sphere) for maximum interaction of miscibility (black arrow indicating NMP as the most preferred solvent or cosolvent) and (B) ternary diagram of HSP parameters and centralized ENO (radius = 9.3), and (C) experimental solubility and HSPiP based predicted solubility (log S) in different excipients

Experimental Solubility Study in HSPiP Predicted Excipients. ENO is associated with limited aqueous solubility and permeability. As a result of this, the drug shows poor antibacterial efficacy and high hygroscopic instability.[4] The solubility of ENO in the predicted excipients was carried out, and the result is portrayed in Figure 3C. Solubility values were estimated in terms of mg/mL and log S so that HSPiP software uses log S values as an input parameter. It is apparent that the solubilities of ENO in Tween 80, C90, and NMP were maximum and these values were observed as 1.5 mg/mL, 2.8 mg/mL, and 6.7 mg/mL, respectively. Among oils, Miglyol 812N showed the highest solubility (5.4 mg/mL). However, this was avoided to select due to color development after 2 h. Therefore, C90 was finally selected as oil in the study. Figure 3C illustrated the pattern of ENO solubility in various excipients. The solubilities of ENO in the predicted C90, Tween 80, and NMP have already been explained in a previous section in terms of Hansen solubility parameters. In brief, improved solubility of ENO is attributed to physicochemical properties of the drug and excipients (C90, Tween 80, and NMP). Cohesive forces, H-bonding ability, polarity (dielectric constant), the dispersive natures of NMP and Tween 80, and lipophilic−lipophilic interaction play together for maximized miscibility/solubility of ENO. In Table 1, the HSP values suggested that Tween 80 showed high solubility, which may be attributed to the dispersive nature (16.8 MPas) and H-bonding ability (9.5 MPas) of Tween 80 and the least differences of

similar HSPs with ENO. A similar pattern was observed with C90 which may be due to fatty acids. In the case of NMP, all three cohesive properties played a major role to solubilize ENO. Figure 2 exhibited the chemical structure of ENO and other excipients. This explained the chemical basis of interaction between ENO and other components, which can be explained on the basis of HSP and H-bonding counts. ENO is a chemically organic acid and contains a heterocyclic ring with N-atom. Both −OH and −NH are responsible for forming H-bonding. Liu et al. concluded based on Hirshfeld surface analysis after forming cocrystals of ENO with various organic acids that the order of intermolecular contact between the polar (H⋯O and H⋯N) and the nonpolar (C⋯C, C⋯H, and others) are consistent with solubility and permeability.[4] Thus, ENO possessed several H-bonding acceptor counts to interact with Tween 80 and C90 for maximum solubility. HSP prediction and the experimental solubility values can be correlated to understand the mechanistic perspective of ENO solubility in these excipients. Moreover, the estimated log S values assisted in helping to understand and establish a relationship between thermodynamic parameters (enthalpy and Gibbs free energy) and experimental solubility (log S) using HSPiP program.

QSAR (Quantitative Structural Activity Relationship) Model Using HSPiP Program. This module of HSPiP program was used to identify trends within a data set (Figure 4A). This statistical module reveals deep insights into HSP
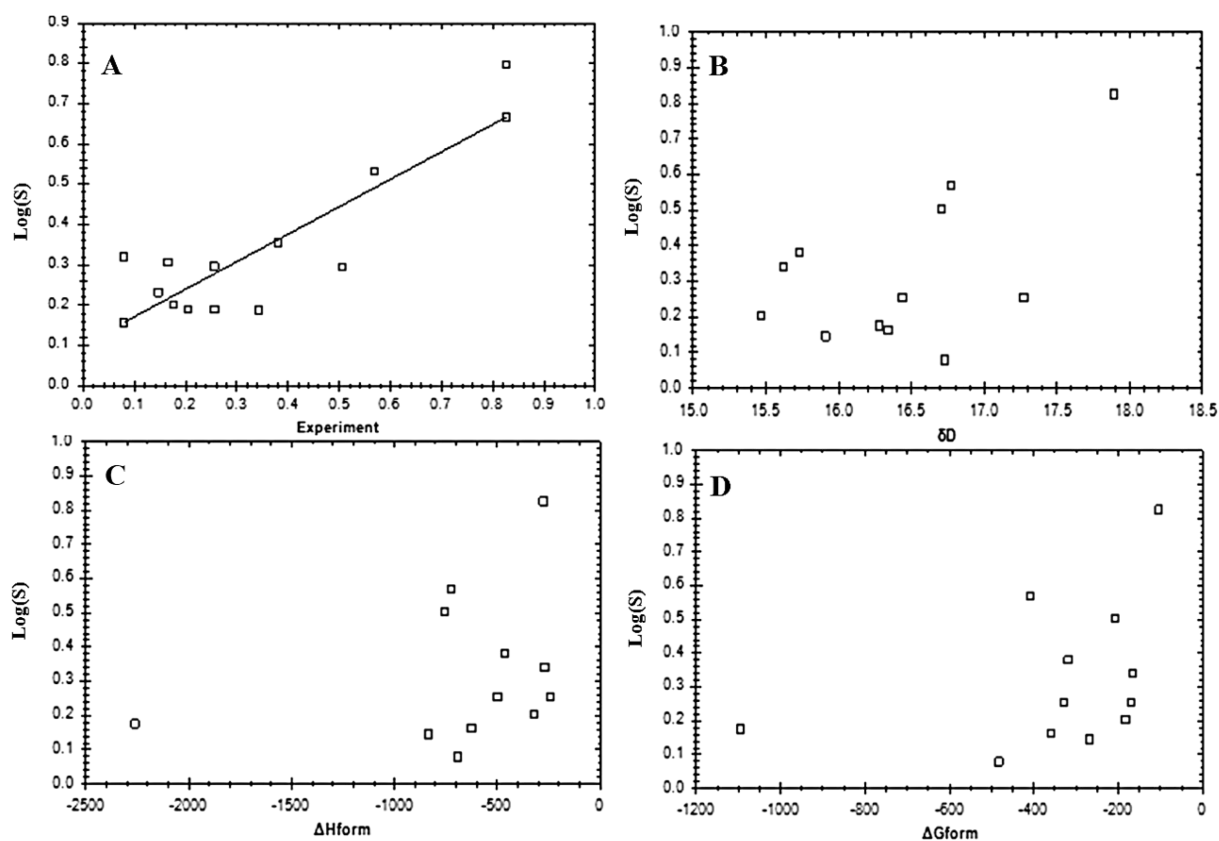
Figure 4. Hansen solubility software based QSAR (quantitative structure–activity relationship in terms of solubility) prediction of studied excipients (solvents, surfactants, and lipids) for log S (experimental solubility values) of ENO and predicted correlation between thermodynamic parameters and HSP parameters. (A) Correlation between the experimental solubility and predicted log S, (B) correlation between log S and Hansen solubility parameter "δ_d" of ENO, (C) correlation predicted between log S and enthalpy of the drug solubility, and (D) correlation between log S and free Gibbs energy of the drug.

about which parameters are the keys to understanding the trend within the data set of log S. Therefore, it does not provide deep mechanistic insights of ENO solubility in the explored excipients due to a lack of theoretical basis. Notably, the module is based on the statistics of good fits ($N = 11$ and the fit to N parameter is 3, at temperature of 25 °C as the default value). The generated polynomial equation was log $S =$ $-1.07 + 0.0809\delta_d + 0.0723\delta_p - 0.0391\delta_h - 9.38 \times 10^{-5}$MVol, wherein MVol is molecular volume ($r^2 = 0.644$). Panels B–D of Figure 4 elicited Hansen solubility software based QSAR (in terms of solubility) prediction of studied excipients (solvents, surfactants, and lipids) for log S (experimental solubility values) of ENO and predicted correlation between thermodynamic parameters (enthalpy and Gibbs free energy) and HSP parameters. We found that all data sets are in good fit with δ_d, whereas other δ_p and δ_h were out of fit (Figure 4B). Similarly, a good correlation was observed between the solubility data set (log S) and two thermodynamic parameters such as ΔH and ΔG, whereas the entropy was out of fit (Figure 4C,D). Thus, the solubility was a spontaneous process in Tween 80, NMP, and C90.

Prepared GNE by Constructing Pseudo-ternary-phase Diagrams (PTDs). To prepare green nanoemulsions, C90, Tween 80, and NMP were selected as major components of the organic phase. Initially, various nanoemulsions were constructed as dictated in pseudoternary phase diagrams (Figure 5). It was mandatory to identify the right proportion of surfactant to cosurfactant ratio (S_{mix}). In ENE1–ENE5, the

content of water was relatively low as compared to organic content (C90, NMP, and Tween 80). Therefore, the blend of organic content was completely homogenized by adding a constant amount of lecithin (7.5%). This resulted in stable water-in-oil ENE1–ENE5 (Table 1). Tween 80 and NMP assisted to stabilize these ENE1–ENE5 after dispersion in bulk aqueous drug solution (transformed into respective o/w types of ENE1–ENE5). Various ratios of S_{mix} were exercised to obtain the most desired pseudoternary phase diagram (delineated with a maximum zone of nanoemulsion. It was clear that cosurfactant and surfactant played a major role to solubilize an aqueous area into organic phase. As depicted in Figure 5A, an equal ratio ($S_{mix} = 1:1$) of surfactant (Tween 80 and lecithin) and cosurfactant (NMP) resulted in limited delineated region, whereas the relative increase in cosurfactant content to surfactant gave rise to an increase in the delineated zone ($S_{mix} = 1:2$). A further increment of cosurfactant content caused slight increase in the delineated area as compared to Figure 5B. Therefore, to ensure the safety concern of surfactants, we could not add further cosurfactant. Thus, S_{mix} at ratio 1:3 was used to formulate ENE1–ENE5. Other ratios (2:1 and 3:1) could not work to get a stable nanoemulsion and dropped from further studies (data not given).[24] Solubilizing properties/emulsification behavior of transcutol-HP (THP) (HLB = 14.5) for C90-oil was facilitated when a blend of lecithin (HLB = 4.2) and THP was used as a combined mix after dispersion/titration with aqueous phase working in tandem.[48] NMP and Tween 80 worked together efficiently
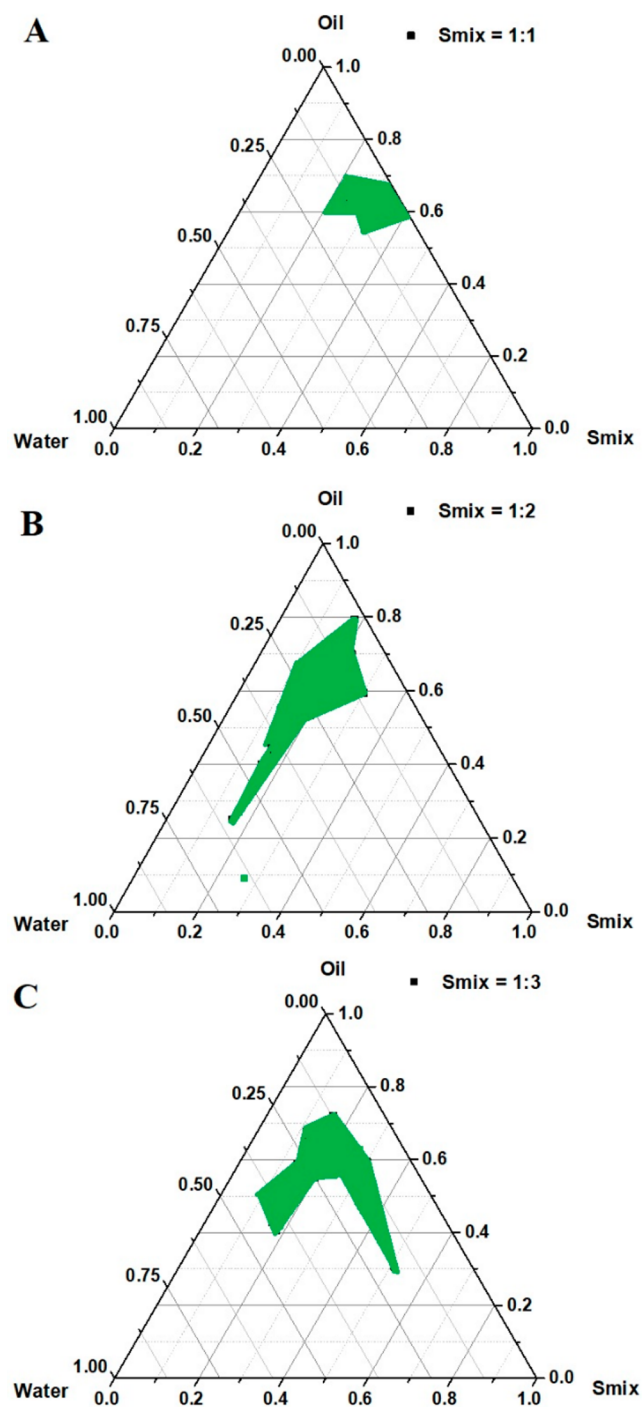
Figure 5. Various constructed pseudoternary phase diagrams. (A) S_{mix} ratio at 1:1, (B) S_{mix} ratio at 1:2 (green dot outside the covered green area indicating unstable nanoemulsion), and (C) S_{mix} ratio at 1:3.

for rapid emulsification of ENE1−ENE5 in the bulk aqueous ENO solution (gave o/w nanoemulsion) with clear transparency. Moreover, biocompatible and lipophilic lecithin served as surfactant for stabilized nanoemulsion before dispersion. Thus, the S_{mix} ratio of 1:3 was selected for (ENE1−ENE5 by changing the amount of oily phase and aqueous phase as per phase diagrams. Table 2 showed a detail of composition of ENE1−ENE5.

Physical Stability under Stressed Thermal and Physical Conditions. To ensure thermodynamic stability of

developed nanoemulsions, it was mandatory to investigate stability against thermal (extreme temperature ranges) and mechanical stress (ultracentrifugation). During transportation, there is chances of phase separation due to physical stress. Table 3 elicited no sign of instability at the end of each

Table 3. Thermodynamic Stability Cycles of the Green Nanoemulsions (Water/T80/NMP/C90)[a]

	Cyclic steps of thermodynamic stability study				
Code	Ultracentrifugation	Cool (4.0 °C)	Freezing (−21.0 °C)	Thawing (45.0 °C)	S_{mix}
ENE1	√	√	√	√	1:3
ENE2	√	√	√	√	1:3
ENE3	√	√	√	√	1:3
ENE4	√	√	√	√	1:3
ENE5	√	√	√	√	1:3

[a]Note: √ represents that nanoemulsion is physically stable under the studied thermal stress and passable for further study.

sequential cycle of cooling and heating. All nanoemulsions passed the test and ensured their ability to withstand high and low temperatures. Moreover, subsequent exposure to ultracentrifugation of ENE1−ENE5 exhibited no signs of any physical instability such as phase separation and creaming. This can be correlated with sufficient quantity of surfactant, right ratio of S_{mix} and Tween 80 of high HLB value for maximum emulsification and firm layer formation around globular surface preventing Ostwald ripening during long-term storage and physical stress. ENE4 and ENE5, having globular size < 100 nm, are very prone to Ostwald ripening due to heterogeneous nature of dispersed globules, weak kinetic barrier, and innate coalescence (<50 nm) on prolonged standing.[49] Therefore, the hurdle can be resolved by selecting the right surfactant and concentration, nature of oil (as depicted in Hansen), oil viscosity, and the molar volume of oil.[49] Notably, it was easy to understand the possible cohesive interaction of the oil phase of ENE1−ENE5 and the drug by the calculated values of HSP parameters as shown in Table 2. Based on the nature and composition of each component (ENE5), we found the values of δ_d, δ_p, and δ_h as 17.46, 9.39, and 14.37, respectively, for ENE5. In this way, ENE5 is capable of interacting with the lipophilic ENO present in the bulk aqueous solution via dispersive nature, polarity, and H-bonding capability for maximized solubility (organic phase as prime site of adsorption). Low globular size may further facilitate the adsorption process and removal efficiency. Thus, a combined blend of lecithin and Tween 80 may have developed a stern layer of S_{mix} at the oil−water interface and substantially reduced surface tension to prevent the probability of globular coalescence while long-term standing.[50]

Characterization Parameters of ENE1−ENE5. Initially, ENE1−ENE5 were prepared and evaluated for size, PDI, ζ potential, viscosity, and RI (Table 4). In general, w/o nanoemulsions are relatively viscous as compared to o/w types of nanoemulsion. Globular sizes of ENE1, ENE2, ENE3, ENE4, and ENE5 ranged from 189, 141, 108, 85, and 61 nm whereas PDI values were observed as 0.53, 0.48, 0.36, 0.29, and 0.18 for the respective ENE1−ENE5. These values suggested that there was progressive reduction in size with an increase in water content in ENE1−ENE5 due to efficient emulsification. ENE1 and ENE5 exhibited maximum and minimum globular sizes among them. The lowest value of PDI of ENE5 further

Table 4. Summary of Characterized Parameters of ENE1−ENE5[a]

	Findings for optimization				
Code	Globular size (nm)	PDI	η (cP)	RI	ζ (mV)
ENE1	189 ± 23	0.53	237.8 ± 12.7	1.442 ± 0.006	−30.8 ± 1.9
ENE2	141 ± 16	0.48	200.1 ± 10.6	1.435 ± 0.005	−28.5 ± 2.0
ENE3	108 ± 17	0.36	167.9 ± 8.5	1.398 ± 0.007	−25.2 ± 1.7
ENE4	85 ± 10	0.29	106.5 ± 6.4	1.367 ± 0.004	−22.7 ± 1.3
ENE5	61 ± 8	0.18	87.3 ± 3.5	1.349 ± 0.002	−22.1 ± 1.5

[a]PDI, polydispersity index; RI = refractive index; ζ, zeta potential; η, viscosity. Data are presented as mean ± standard deviation, $n = 3$.

justified effective and substantial emulsification to significant homogeneous size distribution (PDI = 0.18) as shown in Figure S2. TEM report showed the spherical morphology of ENE5 after dispersion in the bulk aqueous drug solution, suggesting substantial and efficient emulsification within 5 min (the dark spot indicated loaded drug within nanoglobules of green nanoemulsion). This can be correlated with the relative content of water-to-oil concentration (C90). In Table 2, it can be observed that water content increased from 3.5% to 17.5% for ENE1 to ENE5. Similarly, the oil content was reduced from 36.5% to 22.5% for ENE1 to ENE5. Therefore, Tween 80 and lecithin combination (TL) worked efficiently to emulsify the aqueous content into organic phase by reducing surface and interfacial tension as evidenced with the constant reduction in PDI on decreasing relative content of C90 in ENE1−ENE5. Notably, lecithin being lipophilic (HLB = 4) alone may result in bimodal distribution and formation of self-assemblies with a feebly stabilized oil−water interface.[51] C90 has an HLB value of approximately 4 (material leaflet). Therefore, it was imperative to use as combination (TL) with Tween 80 in ENE1−ENE5 as these nanoemulsions are water-in-oil types of nanoemulsion. Thus, initially, lecithin preferentially functioned in w/o before dispersion in the bulk drug solution and vice versa. After dispersion of ENE1−ENE5 (w/o) into the bulk aqueous drug solution, Tween 80 primarily functions as o/w type of emulsifier and results in o/w types of ENE1−ENE5. However, the presence of lecithin (in TL) assists to stabilize the oil−water interface. Globular size and PDI values were further reduced after dispersion. These values were found to be as 124, 97, 72, 65, and 32 nm for ENE1, ENE2, ENE3, ENE4, and ENE5, respectively. This may be attributed to a newly transformed ENE1−ENE5 from w/o to o/w. Lecithin alone results in relatively larger globular sized nanoemulsion as compared to the combination of lecithin and Tween 80.[51] Reduced globular of nanoemulsion after dispersion may be correlated with the decreased interfacial tension when the large number of Tween 80 molecules (compared to lecithin) preferentially adsorbed to the oil−water interface at higher rate and availability in the aqueous phase.[51] Perhaps, lecithin alone is not as effective as Tween 80 in the aqueous system to avoid possible coalescence (Ostwald ripening) during the operational process of preparation (homogenization), storage, and transportation.

The result of ζ potential ranged from 22.1 to 30.8 (−mV) as shown in Table 4. These values are negative which may be enough to establish repulsion among dispersed nanoscale globules for maximized stability. These globules may remain dispersed and minimize the probable chance of coalescence (Ostwald ripening) if stored for long term or during transportation. High values of ζ potential and the negative nature attributed to lipid and lecithin. All nanoemulsions presented Z-potential values (negative) between 20 and 30 mV

and could be considered stable in terms of colloidal interaction against coalescence as lecithin stabilized nanoemulsions (at neutral condition) possessed high negative charge (−50 to −60 mV) to prevent aggregation by generating strong electrostatic repulsion.[52,53] On increasing the surfactant (TL)-to-oil (S/O) ratio (from 0.41 to 0.66), the globular size was substantially reduced from 189 to 61 nm and the result is in agreement with a previous report where a similar pattern was observed on reducing the surfactant-to-oil (S/O) ratio (from 0.43 to 0.6 resulted in average reduction in size from 123 to 115 nm).[53] Thus, a high S/O ratio enforces a reduced interfacial surface tension, small globular size, and high stability.[54]

Viscosity represents rheological behavior of nanoemulsion. The result is illustrated in Table 4, wherein the viscosity values were found to be reduced from ENE1 to ENE5 due to oil concentration (C90). Pure C90 showed viscosity as 21.5 cP close to the reported value (20 cP) (material leaflet). Initially prepared w/o nanoemulsions were relatively more viscous (87.3−237.8 cP) as compared to the respective nanoemulsions after dispersion into the bulk ENO solution. This was obvious due to transformed w/o into o/w nanoemulsion (11.5−23 cP). After dispersion, the interactive terms are dispersed phase volume and S/O ratio as prime factors to decide viscosity. As discussed before, w/o nanoemulsions were more viscous, whereas o/w nanoemulsion elicited a low viscosity. This difference may be correlated to the content of water, C90 content, S/O, and disperse phase volume. ENE5 exhibited low viscosity, low globular size, and being in good consistency for efficient emulsification. After dispersion, the continuous aqueous phase (1/10th dilution) causes phase inversion. In general, w/o types of emulsions take a longer time for emulsification in aqueous medium as compared to o/w type of emulsion.

All of the nanoemulsions ENE1−ENE5 were isotropic and clear. The results of RI are provided in Table 4, wherein the RI values decrease with a decline in C90 content and increase in S/O ratio (from ENE1 to ENE5).[55] This may be correlated with the reduced size of globules from ENE1 to ENE5. Thus, the transparent nature of a nanoemulsion can be associated with optical properties (scattering of light) of isotropic ENE1−ENE5 (less than or ~100 nm) interacting with components.[56] In literature, water is considered as standard reference with RI values of 1.33 being clear and lighter than oil (>1.33). In this study, the obtained values of RI were used to support the findings of globular size, stability, and surface area available for adsorption of lipophilic ENO. The RI value of pure C90 was found as 1.454, which is much greater than those of ENE1−ENE5 and water. Notably, the refractive index values from ENE1 to ENE5 decrease, which may be correlated with the increased content of water (3.5−17.5%) as compared to oil. This may be attributed to the lower value of RI of water as

compared to oil. Similar finding was noticed with C90 when formulated a batch of propranolol-HCl loaded microemulsion was formulated.[57]

Impact of C90 and Water Concentration on Globular Size of ENE1−ENE5. The results of average mean globular size of ENE1−ENE5 is portrayed in Table 4. The size values ranged between 61 and 189 nm from ENE5 to ENE1. The size of ENE1 was found to be relatively higher than that of ENE5, which could be related to the ratio of oil to water content in the nanoemulsion (Figure 6A). Observing the trend of size and PDI values from ENE1 to ENE5, it is apparent that both are progressively decreased, suggesting that ENE5 was the most

Figure 6. Composition (C90 and water content) influencing globular size, viscosity, and PDI of ENE1−ENE5. (A) Composition versus globular size (nm), (B) composition versus viscosity (cP), and (C) impact of composition on PDI and ζ potentials of ENE1−ENE5.

homogeneous and transparent as compared to others. The globular size of the nanoemulsion is an important factor and parameter to decide various functionalities of the nanoemulsion in the present objective. This decides stability, viscosity, transparent and optical properties, physical interaction, and adsorption surface area available for ENO removal from the contaminated water system. Therefore, it was imperative to screen the nanoemulsion with the least globular size among them. Moreover, Figure 6A illustrated the impact of C90 and water content on mean size for ENE1−ENE5. Water had a significant impact as it reduced the size (from 3.5% to 17.5%), whereas the size values were increased on increasing the content of C90 (from 22.5% to 36.5%) in each set of ENE. The result is in good agreement with the previous report (in terms of trend), wherein authors reported removal of indomethacin using green nanoemulsion.[58] Furthermore, transcutol (surfactant) to C90 ratio increases (0.41 for ENE1 and 0.66 for ENE5), which suggested that the oil content of ENE5 was rapidly and efficiently emulsified in the aqueous phase by developing a stable surfactant layer around oil globules to reduce interfacial surface tension by dissipating excess energy at the formed interface layer.[59] There are several other factors to control globular size such as surfactant type, concentration, HLB (hydrophilic−lipophilic balance) values of surfactant and combination blend of surfactant (lecithin and Tween 80), and physical and chemical properties of surfactant and oil. In this section, we focused the impact of C90 and water content on mean globular size and size distribution so that the findings can be correlated with the adsorption percentage of ENO at varied time points. Considering the chemical structure of ENO, it has carboxylic acid with capability to reduce water surface tension through H-bonding ability and increased mole fraction at the adsorbed surface.[60]

Impact of C90 and Water Concentration on Viscosity. In general, the viscosity of an oil based system or nanoemulsion is relatively higher than the pure water system due to the content of oil, surfactant, and other components. An emulsion is supposed to be rapidly emulsified in water after dispersion due to a sufficiently present emulsifier (surfactant and cosurfactant) for homogeneous distribution and nanonization. This frequent emulsification is also related with the viscosity of the system and the oil present in the nanoemulsion. Therefore, it was imperative to assess the viscosity values (flow property of a liquid) of all developed nanoemulsions in the drug bulk aqueous solution. The estimated values are present in Table 4 wherein the values ranged from 87.3 to 237 cP for ENE1−ENE5. Notably, the values 237 and 87 cP correspond to ENE1 and ENE5, which may be correlated to the content of oil C90 (Table 2 and Table 4). Thus, viscosity was substantially affected with the content of C90 oil in the nanoemulsion. There was a consistent decrease in viscosity value (from 237 to 87 cP) with a reduction in C90 concentration (from 36.5% to 22.5%) (Figure 6B). The viscosity value of pure C90 at 20 °C was reported as 20 cP, which is much lower than those of ENE1 and ENE5.[61] Thus, the viscosity of ENE5 is higher than that of pure C90, which may be due to other excipients present in the green nanoemulsion and the type of w/o system. However, the nanoemulsion ENE5 was found to be more suitable in terms of viscosity and flow behavior during dispersion and emulsification. C90 is highly lipophilic due to low HLB (5), and it can be good for the maximized interaction for adsorption of lipophilic ENO. It is noteworthy that the dispersed ENE1−ENE5 in the
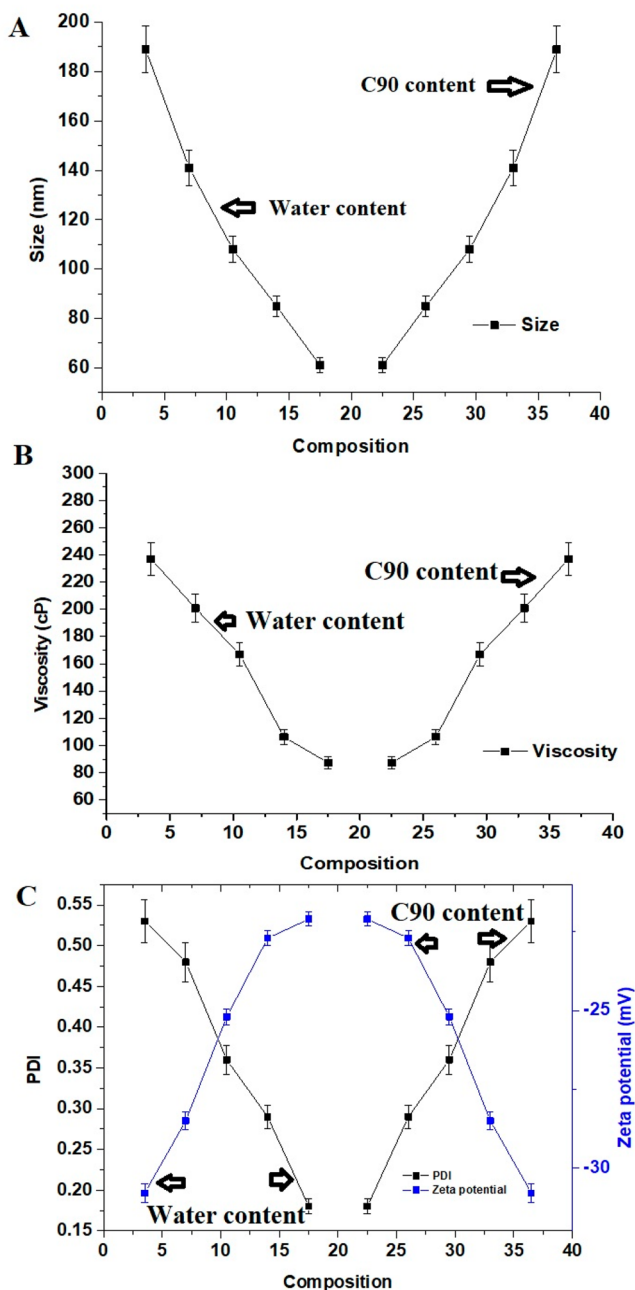
bulk aqueous solution had no significantly different viscosity due to the bulk nature of aqueous medium serving as continuous phase in o/w nanoemulsion.

Figure 6B demonstrated the influence of C90 and water content on viscosity value at constant temperature. In w/o ENE1-ENE5, there were regular reductions in viscosity with reduced content of C90, whereas viscosity was consistently decreasing with increasing content of water. Viscosity may be affected with applied force, while emulsification, by conformation changes under stress, temperature variations, composition, volume fraction of phase, shape and size of dispersed globules, and dipole strength of droplets.[24] However, temperature is the main critical factor to regulate viscosity. Therefore, we attempted to investigate the impact of the prime components on viscosity at constant temperature. The reduction in viscosity in ENE5 also can be correlated with several innate properties of nanoemulsion such as nanonized globular size, volume fraction of water, and transformation of w/o to o/w type. Generally, viscous and gel forms of nanoemulsion may take a longer time of emulsification/ dispersion in water and subsequently poor removal efficiency. For improved removal efficiency of ENO from water, ENE5 could be suitable due to the substantial adsorptive surface, low η for rapidly emulsified, and high stability (stable to face shear-induced stress). Thus, η of ENE1−ENE5 is a valuable parameter to decide on designing selection, composition, and operation processes for the treatment of wastewater at large scale (mixing, handling, storage, and pumping).[62] In this study, we addressed viscosity, globular size, composition, and time of exposure as prime factors to control removal efficiency of ENO, operational process of the designed plant, and the design of an economic plant functional at robust conditions.[62]

Impact of Water and C90 Content on PDI and ζ Potential of ENE1−ENE5. In Figure 6C, the impact of composition on PDI values and ζ potentials has been portrayed. These values are presented in Table 4 for all nanoemulsions. PDI values confirmed the homogeneous and uniform nature of nanoemulsion, whereas negative values of ζ potential can be correlated with fatty components of a C90 and lecithin nature. There may be expected an adsorptive interaction between the drug and globular surface through van der Waals force of attraction (London dispersion force) and H-bonding force interacting between them due to the chemical nature of the drug (acidic functional group and various H-acceptor and H-donor count groups). Considering the chemical structure of the drug, ENO exhibits a zwitterion configuration with −COOH functional group due to quinolone deprotonated (interacting with positive center such as lecithin N-atom), whereas the terminal N(1) of the piperazyl ring of ENO is protonated for electrostatic interaction with negatively charged C90.[63] Thus, these physical interacting forces may be playing together for combined adsorption of the drug to the exposed globular surface. High PDI indicates insufficient content of surfactant, which results into poor emulsification as observed in ENE1.[64] Thus, a low PDI value and high negative ζ potential of ENE5 are quite satisfactory for maintaining physical stability, consistent form, and profound adsorbing surface area available for proficient % RE of ENE5 after dispersion. The C90 and lecithin belong to GRAS (generally regarded as safe) category for developing green nanoemulsions.

Percent Removal Efficiency (%RE) Study and Explanation. Lipid, NMP, and lecithin are prime components of the

developed nanoemulsions and recommended for safe delivery in formulation and U.S. Food and Drug Administration (FDA) approved products. These are safe, biocompatible, and eco-friendly to tailor green nanoemulsion without causing a harmful impact on flora and fauna of an ecosystem. Such cost-effective products possessing high %RE can be easily translated for industrial production and scale up from the laboratory (tech-transfer). The results of % RE have been summarized in Table 5, wherein we found varied values of %

Table 5. Summary of Composition and Contact Time Dependent Removal Efficiency (RE%) of ENE1−ENE5[a]

GNE	%RE		
	5.0 min	10.0 min	15.0 min
ENE5	95.2 ± 10.5	97.3 ± 8.9	99.5 ± 9.2
ENE4	90.1 ± 8.1	92.5 ± 10.4	95.1 ± 7.4
ENE3	82.8 ± 8.2	88.3 ± 6.3	90.4 ± 6.8
ENE2	75.5 ± 8.4	80.7 ± 7.4	85.2 ± 5.1
ENE1	65.8 ± 6.1	70.2 ± 4.8	72.4 ± 7.3

[a]%RE, percent removal efficiency; GNE, green nanoemulsion.

RE due to varied composition and exposure time. Figure 7A demonstrated the relationship of %RE and exposure time (5, 10, and 15 min). At the end of 15 min, ENE1 and ENE5 showed %RE values as 72.4 ± 7.3% and 99.5 ± 9.2%,
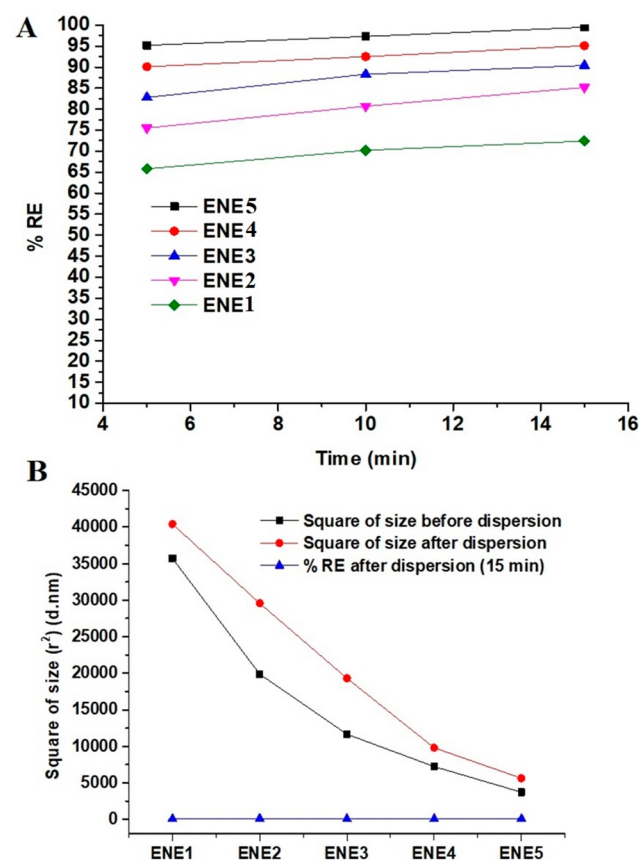
Figure 7. Impact of size and contact time on %RE of ENE1−ENE5: (A) impact of exposure time on percent removal efficiency (%RE) and (B) impact of square of globular size (d, nm) of green nanoemulsion (ENE1−ENE5) on %RE.

respectively, which may be due to the lowest globular size associated with ENE5 providing a maximized adsorption surface for ENO and vice versa (Figure 7B). This adsorption may be attributed to lipophilic−lipophilic interaction, electrostatic interaction, and −COO mediated H-bonding interaction (the terminal N-atom of the piperzyl ring of ENO, uncoordinated −COOH group, and lecithin involved in intermolecular H-bonding).[63,65] To investigate the impact of exposure time, the study was carried out at different time points of contact. We observed a slight increment in %RE values from 5 to 15 min (Table 5).

Considering Hansen parameters of ENO, Tween 80, NMP, and C90, adsorption of ENO with a globular surface can be explained as well. The δ_p values of Tween 80, NMP, and C90 are 16.8, 17.9, and 18.4, which are close to the drug (δ_p = 19.2) for giving the difference values within an acceptable range of miscibility. The δ_h values of Tween 80, NMP, and C90 are 9.5, 7.4, and 9.8, which are close to the drug (δ_h = 9.7) for giving the difference values within acceptable range of miscibility.[28] The Tween 80 was expected to interact mainly through dispersion and H-bonding parameters due to non-ionic nature (δ_p = 6.5). Thus, these interactions (polarity, dispersibility, and H-bonding capability) worked together for preferential adsorption of ENO to the globular surface of nanoemulsion. Furthermore, lipophilic lecithin, C90, and lipophilic ENO were anticipated to interact cohesively for maximum adsorption when dispersed. ENE1−ENE5 (w/o) undergo in situ transformation from w/o to o/w ENE1−ENE5 for hastened comparative intrinsic diffusion of ENO on to C90. These excipients can be understood in terms of polarity, London-dispersion force (apolar), and H-bonding responsible for facilitating interaction between ENO and C90. Tween 80 being highly hydrophilic (HLB = 14) and lipophilic lecithin (HLB = 5) served as surfactant together for generating significantly reduced sized nanoglobules after emulsification in the drug solution through particular (H-bonding capability) intermolecular noncovalent interactions and nonspecific (dipole−dipole, dipole-induced, and instantaneous dipole-induced forces) followed by decreasing surface tension and capillary action while kinetic diffusion in the bulk.[24,66] Relative content of C90 to Tween 80/lecithin decides emulsification efficiency and generated nanoglobules. Conclusively, various factors and mechanistic driving force play simultaneously after dispersion for improved kinetic adsorption of the drug to the available organic surface.[21]

Five factors were studied such as (a) globular size (real d_m values and square of size), (b) contact time up to 15 min, (c) viscosity, and (d) composition (C90 and water). These played a remarkable role on %RE as shown in Figures 6 and 7 (Tables 4 and 5).[62] Considerably low globular size and PDI of ENE5 were 61 nm and 0.18, respectively, suggested they are quite suitable for maximum %RE (99.5%) at the end of 15 min. The combined form of Tween 80 and lecithin substantially fastened emulsification (within 15 min) and stabilized even after dispersion (10 times higher volume). Low size, high ζ potential values, optimal viscosity, and uniform distribution at explored temperature and pH may facilitate diffusion of trace ENO from water phase to organic surface followed by slow molecular rearrangement kinetics.[67] Conclusively, %RE depends upon several other factors (process variables, charged on the drug, pH, and physicochemical properties of excipients), which directly or indirectly had impact on the removal efficiency under experimental conditions.[62] However, we studied the

effect of viscosity, size, composition, and exposure as prime factors controlling %RE of ERN from the aqueous drug solution. Dispersion step results into reduced size o/w nanoemulsion for maximum adsorption surface, reduced viscosity due to phase inversion and high water to C90 volume ratio, and the C90/water volume ratio swiftly varied when dispersed (1:10 dilution). Figure 7C established a relative pattern of the square of size of "ENE1−ENE5" on % RE.

Assessment of Treated Water Using ENE5. It was imperative to negate the presence of ENO in the treated water at the end of 15 min, and the treated water was expected to be free from the drug. UV−vis spectrophotometer and HPLC of the treated water showed no absorbance value and retention peak, respectively, suggesting the absence of the drug from water (data not shown). Chemically, ENO is 1,8-naphthyridine derivative with fluoro substitution at the fifth position of the basic ring. On the other hand, lecithin is rich with phosphorus atom due to phosphate as functional group. To negate this hypothesis, SEM-EDX and elemental analysis (ICP-OES) were the most suitable available advanced tools to identify the drug at the elemental level. The results are presented in Figure 8A,B. The elements "F" and "P" were taken as identifying markers for the drug and lecithin, respectively. Natural hardness of the drinking water is due to carbonate salts of magnesium and calcium. However, other elements may be present such as fluoride, arsenic, lead, copper, mercury, and chromium. It is
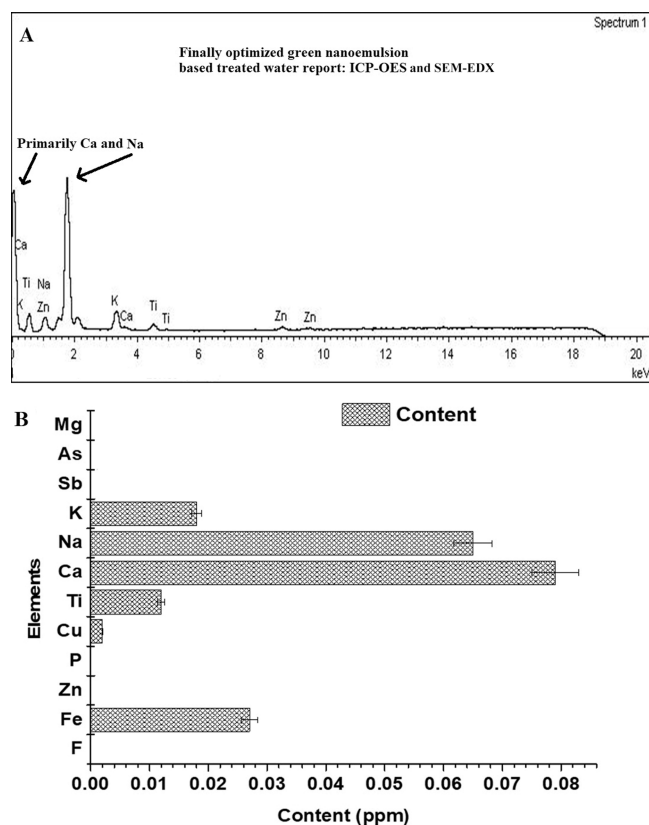
Figure 8. Assessment of the treated water to negate the presence of ENO using (A) SEM-EDX and (B) ICP-OES techniques. The most optimized ENE5 was used to treat water for 15 min and assessed under both techniques to identify the presence of the marker element present in the drug. F- and P-atoms are characteristic elements in ENO and lecithin, respectively.

reported that the acceptable hardness (carbonate hardness) of the drinking water is 300−400 mg/L and TDS value < 500.[68] However, the result showed that there is no fluoride present in SEM-EDX and ICP-OES results. This can be correlated with the absence of the drug or below the detection limit of the used instrument. However, the presence of Mg and Ca suggested the carbonated hardness of the treated water. Similarly, the presence of "P" indicates the trace content of lecithin, which is biocompatible and safe for human body.

In general, the multielement analysis of water is one of the prime applications of ICP-OES to describe the presence or absence of metal or nonmetal elements in drinking water in terms of accuracy, sensitivity, and precision. WHO (World Health Organization) published a guideline as "Guidelines for drinking water quality, 1995" to define a minimum standard and permissible content of inorganic and organic constituents in the drinking water.[69] Potassium as KCl is soluble (344 g/L) in cold water. Iron is the most abundant element in water, and daily consumption required for human is in the range of 10−50 mg/day (FAO/WHO 1988). Its concentration varies as per the source of water such as industrial water (<0.2 mg/L) and black swamp (<0.2 mg/L). Above 0.2 mg/L concentration of iron as ferrous salt causes bitterness in the taste of water. However, the current aquatic life standard for iron content is 1.0 mg/L (1 ppm).[70] Chloride as NaCl is present in public drinking water, and it should not exceed 0.02 ppm set up by WHO. Magnesium (Mg) and calcium (Ca) are significant to detect hardness of water and the set up standards are 75 and 50 ppm by WHO, whereas Cu and Fe are set up as 1 ppm by WHO.[70] Zn should not exceed 3−5 ppm in drinking water as set up by WHO, and recommended hardness of drinking water is 500. The maximum allowable concentration of titanium in drinking water is 0.1 ppm, whereas the smell and taste threshold values were reported (literature) as 4.3 and 3.3 ppm, respectively.[71]

In the sample processing, common elements were ignored to avoid any interference in the result. These are C, O, N, and H. To support the above findings, we further analyzed the treated water using ICP-OES and the results are portrayed in Figure 8B. SEM-EDX report illustrated that the treated water contained Ca, K, and Na at the highest intensity among dissolved salt for causing soft and hard hardness of water. Among the transition metals, Ti, Fe, and Cu were observed which may be due to trace salt present. However, F- and P-atoms were completely absent which may be correlated to very low content below the limit of detection or the absence of the elements (Figure 8A). The abundance of alkali metals (including alkaline earth metals) (Na, K, and Ca) is common due to the natural hardness of water from the dissolved salt. The results of ICP-OE and SEM-EDX were supportive to each other and negated ENO presence. ICP-OES results disclosed that Ca (0.079 ppm), K (0.0018 ppm), Na (0.065 ppm), Ti (0.012), Fe (0.027), P (0.36), and Zn (0.22) were detected in the water whereas a few elements (F, AS, Sb, Cu, and P) were estimated as zero or BDL (below detection limit). These metallic elements are below the set up limit by WHO. Thus, the tailored and optimized ENE5 can be a promised nanocarrier to culminate contaminated water from ENO due to simplicity, effectiveness, rapid process, eco-friendliness, and scalability. To couple with metallic sensor, the approach may be further explored for real time assessment of contamination control and efficiency validation in future advancement. Qin et al. reviewed various transition metal based carbide novel

materials exhibiting interaction with organic compound for multiple applications.[72]

Mechanistic Hypothesis of Removal Process and Pros/Cons Aspect. The drug is a poor aqueous soluble drug due to lipophilic nature. Chemically, it is a mono-carboxylic acid compound of a 1,8-naphthyridine derivative. HSPiP parameter and experimental solubility dictated the explored oil, surfactant, and cosurfactant to tailor green nanoemulsion. The drug is present in trace content (below ppm) in the contaminated water. Therefore, it was hypothesized that ENO and oil can be amalgamated due to lipophilic−lipophilic interaction, HSP parameters based interactions (dispersion force and polarity interaction), and hydrogen bonding interactions (as shown in Tables 1 and 2). The dispersed w/o nanoemulsion (w/o of ENE1−ENE5) into the drug bulk aqueous solution get transformed into respective oil-in-water types (o/w of ENE1−ENE5) of nanoemulsion through emulsification. Surfactant and cosurfactant are capable of stabilizing the transformed nanoemulsion in the studied volume (at room temperature). The dissolved trace content of ENO facilitated to be adsorbed onto the nanoscale exposed the globular surface of the nanoemulsion through fast diffusion (from aqueous medium-to-oil phase) and the described interactive forces (as shown in Figure 9). The process depends
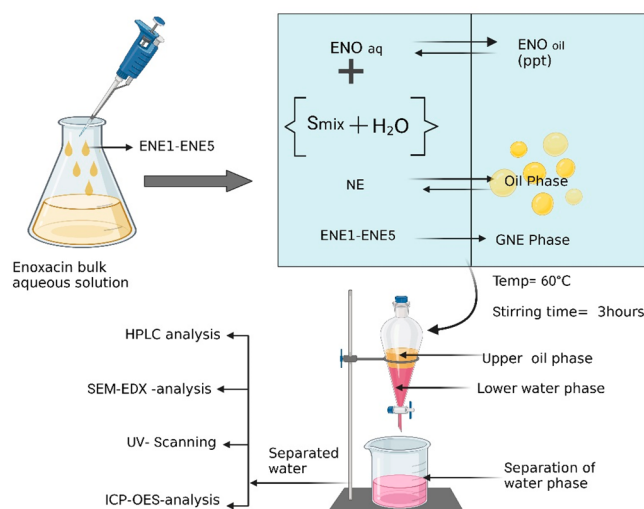
Figure 9. Illustrative representation of the proposed hypothesis for removal of ENO using ENE1−ENE5. The phase separation was thermally induced, and the obtained treated water was analyzed using UV, HPLC, SEM-EDX, and ICP-OES techniques to negate the presence of ENO.

upon various other factors not included in the study. The drug loaded nanoemulsion is heated at high temperature (60 °C) for a long time to crack the nanoemulsion. This results in two phase separation. Both are removed, and the treated water is conformed for the absence of water.

The adopted method is simple, rapid, nontoxic, scalable, and economic. This method is an alternative to the conventional method, wherein trace content of the dissolved drug is unable to be removed due to a low detection limit and instrumental limitation. The method can be set up as a large scale water treatment process after identification of variable factors critical (design related variable process factors and physicochemical properties of nanoemulsion controlling removal efficiency depending upon volume) to control from laboratory to

industrial plant. The method can be designed even for specificity by implementing certain points during the design, development, and process validation. This depends upon physicochemical factors of the drug and the nature of the drug metabolites dissolved in the aqueous system. The developed method is not suitable to remove metallic contaminant due to poor interaction between the organic phase and the dissolved metal ions.

■ CONCLUSION

ENO is the most frequently used antibiotic to control bacterial infections. However, its frequent outflow to the aquatic systems challenges aquatic lives and human health. Conventional methods of its removal from contaminated water are challenged due to low efficiency and toxic byproducts such as chlorination method of the drug degradation. Therefore, the present approach was nondegradation method to treat water using green nanoemulsion (biocompatible excipients such as lecithin and medium chain triglycerides). HSPiP program assisted in screening excipients possessing maximum physicochemical interaction with the drug during adsorption phenomenon after dispersion into the aqueous drug solution. ENE5 was the most suitable product based on composition, size, size distribution, viscosity, and %RE. These products were substantially stable over a wide range of temperature and capable of withstanding physical stress during storage and transportation. It was imperative to identify the major critical factors and variables affecting %RE which can be taken into account during tech transfer from small scale to large scale installation at wastewater treatment plant. These prime variables are composition (oil and water), globular size (low for maximum adsorption surface area), viscosity (improved flow behavior and emulsification), and exposure time for emulsification for the drug. The current method is efficient to remove the trace content of ENO. The proposed approach is simple, rapid, economical, and nontoxic. Conclusively, the approach is promising for controlling ENO contamination from water with high specificity, efficiency, eco-friendliness, and simple installation.

■ ASSOCIATED CONTENT

Ⓢ Supporting Information

The Supporting Information is available free of charge at https://pubs.acs.org/doi/10.1021/acsomega.2c07942.

Thermal behavior of pure ENO using DSC (Figure S1) and globular size distribution intensity and TEM photomicrograph for ENE5 (Figure S2) (PDF)

■ AUTHOR INFORMATION

Corresponding Author

Afzal Hussain − *Department of Pharmaceutics, College of Pharmacy, King Saud University, Riyadh 11451, Saudi Arabia;* ⓞ orcid.org/0000-0002-6275-5375; Phone: +966564591584; Email: amohammed2@ksu.edu.sa

Authors

Syed Sarim Imam − *Department of Pharmaceutics, College of Pharmacy, King Saud University, Riyadh 11451, Saudi Arabia;* ⓞ orcid.org/0000-0002-8913-0826

Mohammad A. Altamimi − *Department of Pharmaceutics, College of Pharmacy, King Saud University, Riyadh 11451, Saudi Arabia*

Mudassar Shahid − *Department of Pharmaceutics, College of Pharmacy, King Saud University, Riyadh 11451, Saudi Arabia*

Osamah Abdulrahman Alnemer − *Department of Pharmaceutics, College of Pharmacy, King Saud University, Riyadh 11451, Saudi Arabia*

Complete contact information is available at:
https://pubs.acs.org/10.1021/acsomega.2c07942

■ ACKNOWLEDGMENTS

■ REFERENCES

(1) Zinner, S. H. Clinical overview of enoxacin. *Clin. Pharmacokinet.* **1989**, *16*, 59−6.

(2) Abell, N. S.; Mercado, M.; Caneque, T.; Rodriguez, R.; Xhemalce, B. Click quantitative mass spectrometry identifies PIWIL3 as a mechanistic target of RNA interference activator enoxacin in cancer cells. *J. Am. Chem. Soc.* **2017**, *139*, 1400−1403.

(3) Mitscher, L. A. Bacterial topoisomerase inhibitors: quinolone and pyridone anti-bacterial agents. *Chem. Rev.* **2005**, *105*, 559−592.

(4) Liu, L.; Zou, D.; Zhang, Y.; Zhang, Q.; Feng, Y.; Guo, Y.; Liu, Y.; Zhang, X.; Cheng, G.; Wang, C.; Zhang, C.; Zhang, L.; Wu, L.; Chang, L.; Su, X.; Duan, Y.; Zhang, Y.; Liu, M. Pharmaceutical salts/cocrystals of enoxacin with dicarboxylic acids: Enhancing in vitro antibacterial activity of enoxacin by improving the solubility and permeability. *Eur. J. Pharm. Biopharm.* **2020**, *154*, 62−73.

(5) Kolar, B.; Arnuš, L.; Jeretin, B.; Gutmaher, A.; Drobne, D.; Durjava, M. K. The toxic effect of oxytetracycline and trimethoprim in the aquatic environment. *Chemosphere* **2014**, *115*, 75−80.

(6) Wise, R. Leading articles antimicrobial resistance: priorities for action. *J. Antimicrob. Chemother.* **2002**, *49* (4), 585−586.

(7) Kolpin, D. W.; Furlong, E. T.; Meyer, M. T.; Thurman, E. M.; Zaugg, S. D.; Barber, L. B.; Buxton, H. T. Pharmaceuticals, hormones, and other organic wastewater contaminants in U.S. streams, 1999−2000: A national re-connaissance. *Environ. Sci. Technol.* **2002**, *36* (6), 1202−1211.

(8) Larsson, D. G. J.; de Pedro, C.; Paxeus, N. Effluent from drug manufactures contains extremely high levels of pharmaceuticals. *J. Hazard. Mater.* **2007**, *148* (3), 751−755.

(9) Zhang, X.; Zhao, H.; Du, J.; Qu, Y.; Shen, C.; Tan, F.; Chen, J.; Quan, X. Occurrence, removal, and risk assessment of antibiotics in 12 wastewater treatment plants from Dalian, China. *Environmental Science and Pollution Research* **2017**, *24* (19), 16478−16487.

(10) Van Doorslaer, X.; Dewulf, J.; Van Langenhove, H.; Demeestere, K. Fluoroquinolone antibiotics: an emerging class of

environmental micropollutants. *Sci. Total Environ.* **2014**, *500*, 250−269.

(11) Pruden, A. Balancing water sustainability and public health goals in the face of growing concerns about antibiotic resistance. *Environ. Sci. Technol.* **2014**, *48* (1), 5−14.

(12) Brain, R. A.; Johnson, D. J.; Richards, S. M.; Sanderson, H.; Sibley, P. K.; Solomon, K. R. Effects of pharmaceutical compounds to *Lemna gibba* using a seven-day static-renewal test. *Environ. Toxicol. Chem.* **2004**, *23* (2), 371−382.

(13) Fasani, E.; Profumo, A.; Albini, A. Structure and medium-dependent photodecomposition of fluoroquinolone antibiotics. *Photochem. Photobiol.* **1998**, *68* (5), 666−67.

(14) Santoke, H.; Tong, A. Y. C.; Mezyk, S. P.; Johnston, K. M.; Braund, R.; Cooper, W. J.; Peake, B. M. UV Photodegradation of Enoxacin in Water: Kinetics and Degradation Pathways. *J. Environ. Eng.* **2015**, *141* (10), No. 04015027.

(15) Arvaniti, O. S.; Frontistis, Z.; Nika, M. C.; Aalizadeh, R.; Thomaidis, N. S.; Mantzavinos, D. Sonochemical degradation of trimethoprim in water matrices: Effect of operating conditions, identification of transformation products and toxicity assessment. *Ultrason. Sonoche* **2020**, *67*, No. 105139.

(16) Liu, Q. T.; Williams, H. E. Kinetics and degradation products for direct photolysis of beta-blockers in water. *Environ. Sci. Technol.* **2007**, *41* (3), 803−810.

(17) Li, W.; Lu, S.; Qiu, Z.; Lin, K. Clofibric acid degradation in UV254/H$_2$O$_2$ process: Effect of temperature. *J. Hazard. Mater.* **2010**, *176* (1−3), 1051−1057.

(18) Homem, V.; Santos, L. Degradation and Removal Methods of Antibiotics from Aqueous Matrices-a Review. *J. Environ. Manage.* **2011**, *92* (10), 2304−2347.

(19) Li, M.; Wei, D.; Du, Y. Acute Toxicity Evaluation for Quinolone Antibiotics and Their Chlorination Disinfection Processes. *J. Environ. Sci.* **2014**, *26* (9), 1837−1842.

(20) Arvaniti, O. S.; Stasinakis, A. S. Review on the occurrence, fate and removal of per-fluorinated compounds during wastewater treatment. *Sci. Total Environ.* **2015**, *524−525*, 81−92.

(21) Shakeel, F.; Haq, N.; Alanazi, F. K.; Alsarra, I. A. Development of dilutable green nanoemulsions for removal of Eriochrome black T from aqueous solution and optimization by Box−Behnken design. *J. Mol. Liq.* **2014**, *196*, 340−347.

(22) Mahdi, W. A.; Hussain, A.; Bukhari, S. I.; Alshehri, S.; Singh, B.; Ali, N. Removal of clarithromycin from aqueous solution using water/ triton X-100/ ethanol/ olive oil green nanoemulsion method. *Journal of Water Process Engineering* **2021**, *40*, 101973.

(23) Hussain, A.; Mahdi, W. A.; Alshehri, S.; Bukhari, S. I.; Almaniea, M. A. Application of green nanoemulsion for elimination of rifampicin from a bulk aqueous solution. *Int. J. Environ. Res. Public Health* **2021**, *18*, 5835.

(24) Hussain, A.; Afzal, O.; Altamimi, A. S. A.; Ali, R. Application of green nanoemulsion to treat contaminated water (bulk aqueous solution) with azithromycin. *Environ. Sci. Pollut. Res.* **2021**, *28*, 61696−61706.

(25) Zaini, E.; Sumirtapura, Y. C.; Halim, A.; Fitriani, L.; Soewandhi, S. N. Formation and Characterization of Sulfamethoxazole-Trime-thoprim Cocrystal by Milling Process. *J. Appl. Pharm. Sci.* **2017**, *7* (12), 169−173.

(26) Hussain, A.; Shakeel, F.; Singh, S. K.; Alsarra, I. A.; Faruk, A.; Alanazi, F. K.; Christoper, G. V. P. Solidified SNEDDS for the oral delivery of rifampicin: Evaluation, proof of concept, in vivo kinetics, and in silico GastroPlus^{TM} simulation. *Int. J. Pharm.* **2019**, *566*, 203−217.

(27) Afzal, O.; Alshammari, H. A.; Altamimi, M. A.; Hussain, A.; Almohaywi, B.; Altamimi, A. S. A. Hansen solubility parameters and green nanocarrier based removal of trimethoprim from contaminated aqueous solution. *J. Mol. Liq.* **2022**, *361*, 119657.

(28) De La Peña-Gil, A.; Toro-Vazquez, J. F.; Rogers, M. A. Simplifying Hansen Solubility Parameters for Complex Edible Fats and Oils. *Food Biophysics* **2016**, *11* (3), 283−291.

(29) Sun, Y. X.; Ding, Y. P.; He, X. J.; Zhao, L. M. Determination of enoxacin in human plasma by high-performance liquid chromatography and its pharmacokinetics. *Chin. J. Antibiot.* **2006**, *31* (12), 758−760.

(30) Hansen, C. M. *Hansen Solubility Parameters: A User's Handbook*, 2nd ed.; CRC Press, Boca Raton, FL, USA, 2006.

(31) Khalil, A. M. E.; Memon, F. A.; Tabish, T. A.; Fenton, B.; Salmon, D.; Zhang, S.; Butler, D. Performance evaluation of porous graphene as filter media for the removal of pharmaceutical/emerging contaminants from water and wastewater. *Nanomaterials (Basel)* **2021**, *11* (1), 79.

(32) Luo, Z.; Yu, G.; Han, X.; Yang, T.; Ji, Y.; Huang, H.; Wang, G.; Liu, Y.; Sun, W. Prediction of the pharmacokinetics and pharmacodynamics of topiroxostat in humans by integrating the physiologically based pharmacokinetic model with the drug-target residence time model. *Biomedicine & Pharmacotherapy* **2020**, *121*, 109660.

(33) Hussain, A.; Singh, S. K.; Singh, N.; Prasad Verma, P. R. In vitro−in vivo−in silico simulation studies of anti-tubercular drugs doped with a self-nanoemulsifying drug delivery system. *RSC Adv.* **2016**, *6* (95), 93147−93161.

(34) Bellalta, P.; Troncoso, E.; Zúñiga, R. N.; Aguilera, J. M. Rheological and microstructural characterization of WPI-stabilized O/ W emulsions exhibiting time-dependent flow behavior. *LWT - Food Science and Technology* **2012**, *46* (2), 375−381.

(35) Khodier, S. A. Refractive index of standard oils as a function of wavelength and temperature. *Optics & Laser Technology* **2002**, *34* (2), 125−128.

(36) Laxmi, M.; Bhardwaj, A.; Mehta, S.; Mehta, A. Development and characterization of nanoemulsion as carrier for the enhancement of bioavailability of artemether. *Artificial Cells, Nanomedicine, and Biotechnology* **2015**, *43* (5), 334−344.

(37) Wei, Z.; Spinney, R.; Ke, R.; Yang, Z.; Xiao, R. Effect of pH on the sonochemical degradation of organic pollutants. *Environmental Chemistry Letters* **2016**, *14* (2), 163−182.

(38) Saleeman, R.; Carter, J. F. Instrumental analysis of explosive: Forensic Sciences (Explosive). In *Encyclopedia of Analytical Science*, 2nd ed.; Elsevier, 2005; pp 400−406. DOI: 10.1016/B0-12-369397-7/00198-9.

(39) Odenigbo, C.; Makonnen, Y.; Asfaw, A.; Anastassiades, T.; Beauchemin, D. Towards the use of ICP-OES for the elemental analysis of organic compounds such as glucosamine. *Journal of Analytical Atomic Spectrometry* **2014**, *29* (3), 454.

(40) Van der Voet, G. B.; Sarafanov, A.; Todorov, T. I.; Centeno, J. A.; Jonas, W. B.; Ives, J. A.; Mullick, F. G. Clinical and Analytical Toxicology of Dietary Supplements: A Case Study and a Review of the Literature. *Biological Trace Element Research* **2008**, *125* (1), 1−12.

(41) Sehar, S.; Naz, I.; Ali, N.; Ahmed, S. Analysis of elemental concentration using ICP-AES and pathogen indicator in drinking water of Qasim Abad, District Rawalpindi, Pakistan. *Environmental Monitoring and Assessment* **2013**, *185* (2), 1129−1135.

(42) Afzal, A. M.; Rasool, M. H.; Waseem, M.; Aslam, B. Assessment of heavy metal tolerance and biosorptive potential of Klebsiella variicola isolated from industrial effluents. *AMB Express* **2017**, *7* (1), 1−9.

(43) Van Doorslaer, X.; Dewulf, J.; Van Langenhove, H. D.; Demeestere, K. Fluoroquinolone antibiotics: An emerging class of environmental micropollutants. *Sci. Total Environ.* **2014**, *500−501*, 250−269.

(44) Computed Properties. *Pubchem*, National Center for Biotechnology Information, National Institutes for Health, Bethesda, MD, USA; https://pubchem.ncbi.nlm.nih.gov/compound/ Enoxacin#section=Computed-Properties (accessed 2022-10-17].

(45) Mohammadian, E.; Rahimpour, E.; Martinez, F.; Jouyban, A. Budesonide solubility in polyethylene glycol 400 + water at different temperatures: Experimental measurement and mathematical modelling. *J. Mol. Liq.* **2019**, *274*, 418−425.

(46) Ukai, H.; Iwasa, K.; Deguchi, T.; Morishita, M.; Katsumi, H.; Yamamoto, A. Enhanced Intestinal Absorption of Insulin by Capryol

90, a Novel Absorption Enhancer in Rats: Implications in Oral Insulin Delivery. *Pharmaceutics* **2020**, *12* (5), 462.

(47) Mathieu, D. Pencil and Paper Estimation of Hansen Solubility Parameters. *ACS Omega* **2018**, *3* (12), 17049−17056.

(48) Shah, B. M.; Misra, M.; Shishoo, C. J.; Padh, H. Nose to brain microemulsion-based drug delivery system of rivastigmine: formulation and ex-vivo characterization. *Drug Delivery* **2015**, *22*, 918−930.

(49) Wooster, T. J.; Golding, M.; Sanguansri, P. Impact of Oil Type on Nanoemulsion Formation and Ostwald Ripening Stability. *Langmuir* **2008**, *24* (22), 12758−12765.

(50) Pal, R. Modeling the viscosity of concentrated nanoemulsions and nanosuspensions. *Fluids* **2016**, *1* (2), 11.

(51) Fuentes, K.; Matamala, C.; Martínez, N.; Zúñiga, R. N.; Troncoso, E. Comparative Study of Physicochemical Properties of Nanoemulsions Fabricated with Natural and Synthetic Surfactants. *Processes* **2021**, *9* (11), 2002.

(52) Bot, F.; Cossuta, D.; O'Mahony, J. A. Inter-relationships between composition, physicochemical properties and functionality of lecithin ingredients. *Trends Food Sci. Technol.* **2021**, *111*, 261−270.

(53) Mehmood, T.; Ahmed, A.; Ahmed, Z.; Ahmad, M. S. Optimization of soya lecithin and Tween 80 based novel vitamin D nanoemulsions prepared by ultrasonication using response surface methodology. *Food Chem.* **2019**, *289*, 664−670.

(54) Homayoonfal, M.; Khodaiyan, F.; Mousavi, S. M. Walnut oil nanoemulsion: Optimization of the emulsion capacity, cloudiness, density, and surface tension. *J. Dispersion Sci. Technol.* **2014**, *35* (5), 725−733.

(55) Saberi, A. H.; Fang, Y.; McClements, D. J. Fabrication of vitamin E-enriched nanoemulsions by spontaneous emulsification: effect of propylene glycol and ethanol on formation, stability, and properties. *Food Res. Int.* **2013**, *54* (1), 812−820.

(56) Kotta, S.; Khan, A. W.; Ansari, S. H.; Sharma, R. K.; Ali, J. Formulation of nanoemulsion: a comparison between phase inversion composition method and high-pressure homogenization method. *Drug Delivery* **2015**, *22*, 455−466.

(57) Olariu, I.; Coneac, G.; Vlaia, L.; Vlaia, V.; Anghel, D. F.; Ilie, C.; Popoiu, C.; Lupuleasa, D. Development and evaluation of microemulsion-based hydrogel formulations for topical delivery of propranolol hydrochloride. *Dig. J. Nanomater. Biostruct.* **2014**, *9* (1), 395−412.

(58) Shakeel, F.; Haq, N.; Sumague, T. S.; Alanazi, F. K.; Alsarra, I. A. Removal of indomethacin from aqueous solution using multicomponent green nanoemulsions. *J. Mol. Liq.* **2014**, *198*, 329−333.

(59) Garti, N. A new approach to improved stability and controlled release in double emulsions by the use of graft-combpolymeric amphiphiles. *Acta Polym.* **1998**, *49*, 606−616.

(60) Hyvärinen, A. P.; Lihavainen, H.; Gaman, A.; Vairila, L.; Ojala, H.; Kulmala, M.; Viisanen, Y. Surface Tensions and Densities of Oxalic, Malonic, Succinic, Maleic, Malic, andcis-Pinonic Acids. *Journal of Chemical & Engineering Data* **2006**, *51* (1), 255−260.

(61) *Capryol 90*. Gattefossé, Saint-Priest, France; https://www.gattefosse.com/pharmaceuticals-products/capryol-90. (Accessed on November 19, 2022).

(62) Alliod, O.; Messager, L.; Fessi, H.; Dupin, D.; Charcosset, C. Influence of viscosity for oil-in-water and water-in-oil nanoemulsions production by SPG premix membrane emulsification. *Chem. Eng. Res. Des.* **2019**, *142*, 87−99.

(63) Yu, L. C.; Lai, L.; Liu, S. L.; Xia, Y. Syntheses and crystal structure studies of two zinc complexes of enoxacin. *J. Coord. Chem.* **2009**, *62* (16), 2616−2622.

(64) Jakab, G.; Fülöp, V.; Bozó, T.; Balogh, E.; Kellermayer, M.; Antal, I. Optimization of quality attributes and atomic force microscopy imaging of reconstituted nanodroplets in baicalin loaded self-nanoemulsifying formulations. *Pharmaceutics* **2018**, *10*, 275.

(65) Singh, S.; Pathak, K.; Bali, V. Product Development Studies on Surface-Adsorbed Nanoemulsion of Olmesartan Medoxomil as a Capsular Dosage Form. *AAPS PharmSciTech* **2012**, *13* (4), 1212−1221.

(66) Abdallah, D. J.; Weiss, R. G. n-Alkanes Gel n-Alkanes (and Many Other Organic Liquids). *Langmuir* **2000**, *16*, 352−355.

(67) de Morais, J. M.; dos Santos, O. D. H.; Delicato, T.; da Rocha-Filho, P. A. Characterization and evaluation of electrolyte influence on canola oil/water nano-emulsion. *J. Dispers. Sci. Technol.* **2006**, *27* (7), 1009−1014.

(68) Sharma, S.; Bhattacharya, A. Drinking water contamination and treatment techniques. *Applied Water Science* **2017**, *7* (3), 1043−1067.

(69) World Health Organization; International Programme on Chemical Safety. *Guidelines for drinking water quality*, 2nd ed.; Health criteria and other supporting information, Vol. 2; World Health Organization (WHO), 1998. https://apps.who.int/iris/handle/10665/38551 [accessed on 2022-10-10].

(70) Kumar, M.; Puri, A. A review of permissible limits of drinking water. *Indian Journal of Occupational and Environmental Medicine* **2012**, *16* (1), 40.

(71) Dong, S. D.; Chen, C. Z.; Li, D. M.; Sun, Y. S. A study of hygienic standard for titanium in the source of drinking water. *Zhonghua Yufang Yixue Zazhi* **1993**, *27* (1), 26−28.

(72) Qin, T.; Wang, Z.; Wang, Y.; Besenbacher, F.; Otyepka, M.; Dong, M. Recent Progress in Emerging Two-Dimensional Transition Metal Carbides. *Nano-Micro Letters* **2021**, *13*, 183.